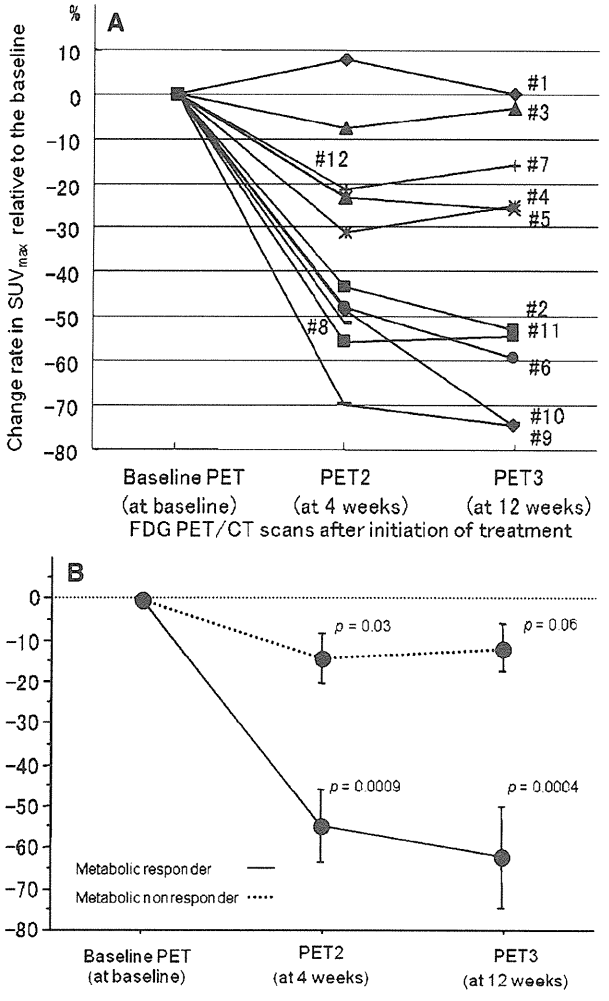

Fig. 2 Reduction in SUV_{max} of primary breast cancers measured by FDG PET/CT during neoadjuvant letrozole therapy. **a** Plots for all 12 tumors. In two tumors (nos. *8* and *12*), only baseline PET and PET2 were performed. A clear threshold at the points of PET2 appears to exist between tumor no. 5 (31.4% decrease) and tumor no. 2 (43.4% decrease). **b** Plots for average % reductions in SUV_{max} in metabolic responders and metabolic non-responders. Metabolic responders and metabolic nonresponders were tentatively defined as tumors with 40% or more reduction or with less than 40% reduction, respectively, in SUV_{max} at PET2 compared with SUV_{max} at baseline PET. The average reduction in SUV at PET2 compared with baseline PET was 60.9% [±21.3 standard deviation (SD)] in metabolic responders ($p = 0.0009$) and 14.2% (±12.0 SD) in metabolic nonresponders ($p = 0.03$). Likewise, the average reduction in SUV_{max} at PET3 compared with baseline PET was 64.5% (±18.7 SD) in metabolic responders ($p = 0.0004$) and 16.7% (±14.1 SD) in metabolic nonresponders ($p = 0.06$)

Cell cycle response measured by the Ki67 labeling index

Five of six metabolic responders showed a marked decrease in the Ki67 labeling index at 2 weeks and/or at surgery compared with the index at baseline (Fig. 5). In contrast, the degree of decrease in the Ki67 labeling index was relatively small or inverse in six metabolic nonresponders (Fig. 5). Compared with the baseline Ki67 labeling index, metabolic responders showed a significant decrease in the labeling index during therapy by Wilcoxon signed-ranks test: mean 62.9% (±35.9 SD) after 2 weeks of treatment ($Z = 2.0$, $p = 0.04$) and mean 91.7% (±10.7 SD) at surgery ($Z = 2.2$, $p = 0.03$). Conversely, metabolic nonresponders showed no significant decrease in labeling index by the Wilcoxon signed-ranks test: mean 9.8% (±26.3 SD) after 2 weeks of treatment ($Z = 0.8$, $p = 0.4$) and mean −49.5% (±138.8 SD) at surgery ($Z = 0.5$, $p = 0.6$) (Fig. 5). That analysis supported the validity of 40% SUV_{max} reduction of the cutoff value between the metabolic responders and the metabolic nonresponders.

Discussion

This study revealed that FDG PET/CT measurements were correlated with cell-cycle response to neoadjuvant letrozole in HR-positive breast cancers. When the 12 tumors were divided into metabolic responders and nonresponders according to a tentative cutoff value of 40% reduction in SUV_{max} at PET2 compared with the baseline PET, the former showed a further decline of SUV_{max} at PET3 ($p = 0.0004$), whereas the latter showed no significant change of SUV_{max} at PET3 ($p = 0.06$). On the contrary, the assessment of morphological response did not reveal significant differences between pre-therapeutic and post-therapeutic tumor sizes in both metabolic responders ($p = 0.3$) and nonresponders ($p = 0.5$).

Previous studies have concluded that 3 or 4 months of treatment with neoadjuvant letrozole for postmenopausal patients with breast cancer provides incremental clinical benefit for these patients. However, these studies did not determine the optimum duration of treatment. Therefore, Krainick-Strobel et al. [25] investigated the optimal duration of neoadjuvant letrozole therapy in postmenopausal patients with HR-positive breast cancer. Their data suggested that prolonged treatment for up to 8 months could result in greater tumor shrinkage compared with treatment for 4 months. From the present observations of metabolic response as well as a decrease in the Ki67 labeling index after the initiation of endocrine therapy, we suggest prolonged treatment duration of neoadjuvant letrozole therapy for 3 months or longer might be effective, especially in metabolic responders.

In recent studies of neoadjuvant chemotherapy, early metabolic response monitored by serial FDG PET scans after one or two cycles of chemotherapy was correlated with the pathological response of primary breast cancer [17, 18, 26–28]. With regard to pathological response in

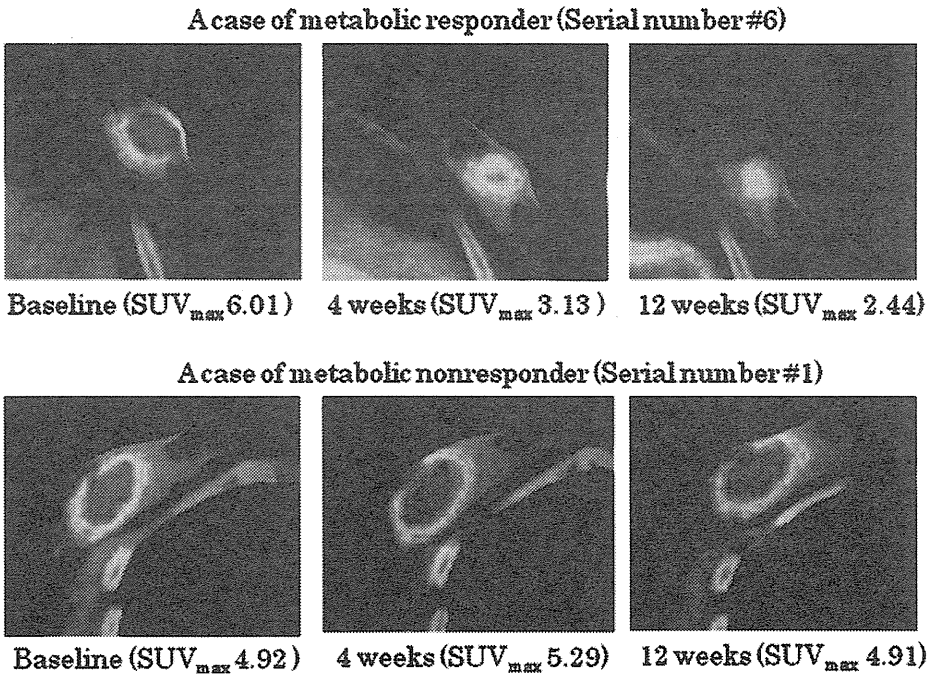

Fig. 3 Transversal slice images from FDG PET/CT of breast lesions before neoadjuvant letrozole therapy (*left*), at 4 weeks after the initiation of therapy (*middle*), and after 12 weeks of therapy and prior to surgery (*right*). A tumor classed as a metabolic responder (serial no. 6; *upper row*) shows SUV_{max} values of 6.01 (*left*), 3.13 (*middle*), and 2.44 (*right*). A tumor classed as a metabolic nonresponder (serial no. 1; *lower row*) shows SUV_{max} values of 4.92 (*left*), 5.29 (*middle*), and 4.91 (*right*)

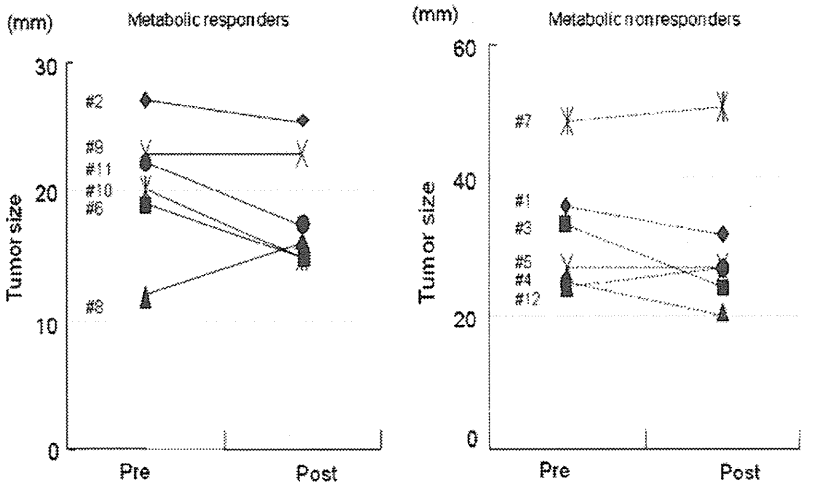

Fig. 4 Box plot of tumor size before and after neoadjuvant letrozole therapy of hormone-receptor-positive primary breast cancers. Among the six tumors with a metabolic response, four (67%) showed a decrease in tumor size, whereas two (33%) showed no change or an increase in tumor size. Among the six tumors with a metabolic nonresponse, three (50%) showed a decrease in tumor size, whereas the other three (50%) showed an increase in tumor size. Tumors with a metabolic response showed an average 3.2-mm reduction in size, ranging from 0.5 to 5.9 mm ($p = 0.3$), and tumors with a metabolic nonresponse also showed an average 3.2-mm reduction in size, ranging from −4.4 to 10.4 mm ($p = 0.5$). Each serial number in the box plot corresponds to a tumor

neoadjuvant endocrine therapy, it was shown that histological criteria for evaluation of therapeutic effect remained good not only for neoadjuvant chemotherapy, but also for neoadjuvant endocrine therapy [29]. In the present study, neither tumors of metabolic responders nor those of metabolic nonresponders achieved remarkable changes of grade 2 or 3 after surgery. However, the therapeutic effect of grade 1b was observed only in metabolic responders, and, if a larger number of cases were studied, metabolic response may be able to predict pathological response to neoadjuvant endocrine therapy.

Cell-cycle responses or decreases in the Ki67 labeling index both after 2 weeks of endocrine therapy and at surgery in comparison with the labeling index at the baseline were significantly greater in metabolic responders than in metabolic nonresponders. These data suggest that the

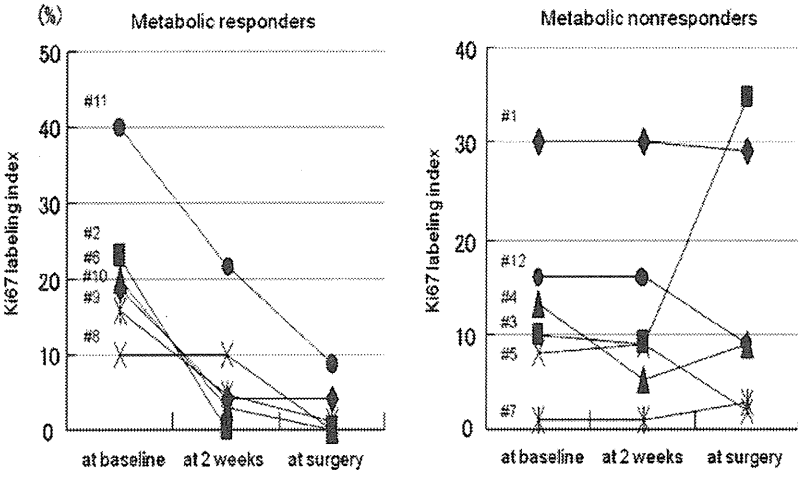

Fig. 5 Box plot of the Ki67 labeling index in primary breast cancers at baseline, at 2 weeks after initiation of neoadjuvant letrozole therapy, and at surgery. Five of six metabolic responders showed a marked decrease in the Ki67 labeling index at 2 weeks and/or at surgery compared with the index at baseline. In contrast, the degree of decrease in the Ki67 labeling index was relatively small or inverse in six metabolic nonresponders. Metabolic responders showed an average 62.9% (±35.9% SD) decrease in the Ki67 labeling index at 2 weeks after initiation of therapy ($z = 2.0, p = 0.04$) and an average 91.7% (±10.7% SD) decrease at surgery ($z = 2.2$, $p = 0.03$), compared with baseline. Metabolic nonresponders showed no significant change in the Ki67 labeling index at 2 weeks after initiation of therapy ($z = 0.8, p = 0.4$) or at surgery ($z = 0.5, p = 0.6$) compared with baseline. These analyses were performed by Wilcoxon signed-ranks test. Each serial number corresponds to a tumor

metabolic response of tumors to endocrine therapy might be underpinned by this marked suppression of proliferative activity in the 2 weeks after initiation of treatment.

Dowsett et al. [8] compared neoadjuvant endocrine therapy using anastrozole or tamoxifen or the combination of anastrozole plus tamoxifen in 158 patients with hormone receptor-positive primary disease and reported that the higher Ki67 labeling index after 2 weeks of endocrine therapy was significantly associated with shorter recurrence-free survival. However, measurement of the tumor Ki67 labeling index has limitations in that tissue samples obtained by means of CNB might be too small for proper assessment, since Ki67 expression in tumors may not be evenly distributed [3, 6]. Because tumor SUV_{max} values closely correlate with proliferative activity, FDG PET appears to be a less invasive and more easily applicable method for assessing response than measurement of the Ki67 labeling index in CNB samples.

Currently, a prospective clinical trial of neoadjuvant endocrine therapy using FDG PET and 16 alpha ^{18}F-fluoroestradiol (FES) PET, which uses a radio-labeled estradiol tracer as a marker for hormone sensitivity of breast cancer, to assess response is ongoing (see ClinicalTrials.gov, http://clinicaltrials.gov). The trial (NCT00362973) will investigate whether FDG PET and FES PET are useful for evaluating early response to treatment in patients receiving hormone therapy or trastuzumab for HR-positive primary breast cancer. Patients will undergo PET scans at baseline and at 2 weeks after the initiation of neoadjuvant endocrine therapy. CNB is also performed after 2 weeks of therapy to monitor tumor proliferation by the Ki67 index. The trial will assess the predictive value of FDG PET and/or FES PET for determining endocrine sensitivity in patients with HR-positive breast cancer.

This study has certain limitations. The chief weakness is a small number of patients. A much larger study with long-term follow-up would be necessary to determine directly whether FDG PET/CT has any role to play in the early prediction of hormone responsiveness. Second, we failed in a simultaneous comparison between Ki67 levels of the biopsy and SUV measured by PET at 2 weeks after the initiation of treatment because of patient availability. Third, we were only able to set tentatively the optimal cutoff of SUV_{max} change for differentiating responders and non-responders due to the lack of comparison data between metabolic response and clinicopathologic outcomes.

Recently, some investigators proposed the concept of a "cell cycle response" as a post-treatment endpoint based on the Ki67 value with 1% or less in the infiltrating component of the tumor that might have properties similar to the pathological complete response used as an endpoint in trials of neoadjuvant chemotherapy [30, 31]. Therefore, it is of note that when tumors with 1% or less of posttherapeutic Ki67 value are considered as having a favorable outcome, receiver operating characteristic (ROC) curve analysis provided a 43.4% decrease in SUV_{max} as the optimized cutoff value with sensitivity of 100% and specificity of 87.5%. This cutoff value was almost

consistent with the tentative cutoff SUV of 40% made by this study.

In conclusion, this pilot study demonstrated that an early reduction in SUV_{max} at 4 weeks after initiation of neoadjuvant letrozole compared with the baseline SUV_{max} was closely associated with reduction in Ki67 labeling index. Therefore, we suggest that incorporation of FDG PET or PET/CT scans into assessment protocols could be feasible for accurate evaluation of the endocrine responsiveness of tumor cells.

Acknowledgments This work was supported by grants for the promotion of Defense Medicine from the Ministry of Defense, Japan, and from the Department of Breast Oncology of the International Medical Center at Saitama Medical University. The authors would like to thank Takaaki Suzuki for providing data related to previously published studies.

Conflict of interest statement The authors declare that they have no competing interests.

References

1. Kaufmann M, von Minckwitz G, Bear HD, Buzdar A, McGale P, Bonnefoi H, et al. Recommendations from an international expert panel on the use of neoadjuvant (primary) systemic treatment of operable breast cancer: new perspectives 2006. Ann Oncol. 2007;18(12):1927–34.
2. Macaskill EJ, Renshaw L, Dixon JM. Neoadjuvant use of hormonal therapy in elderly patients with early or locally advanced hormone receptor-positive breast cancer. Oncologist. 2006;11(10):1081–8.
3. Ellis MJ, Ma C. Letrozole in the neoadjuvant setting: the P024 trial. Breast Cancer Res Treat. 2007;105(Suppl 1):33–43.
4. Smith IE, Dowsett M, Ebbs SR, Dixon JM, Skene A, Blohmer JU, et al. Neoadjuvant treatment of postmenopausal breast cancer with anastrozole, tamoxifen, or both in combination: the immediate preoperative anastrozole, tamoxifen, or combined with tamoxifen (IMPACT) multicenter double-blind randomized trial. J Clin Oncol. 2005;23(22):5108–16.
5. Takei H, Suemasu K, Inoue K, Saito T, Okubo K, Koh J, et al. Multicenter phase II trial of neoadjuvant exemestane for postmenopausal patients with hormone receptor-positive, operable breast cancer: Saitama Breast Cancer Clinical Study Group (SBCCSG-03). Breast Cancer Res Treat. 2008;107(1):87–94.
6. Ellis MJ. Neoadjuvant endocrine therapy for breast cancer: more questions than answers. J Clin Oncol. 2005;23(22):4842–4.
7. Dowsett M, Smith IE, Ebbs SR, Dixon JM, Skene A, Griffith C, et al. Proliferation and apoptosis as markers of benefit in neoadjuvant endocrine therapy of breast cancer. Clin Cancer Res. 2006;12(3 Pt 2):1024s–30s.
8. Dowsett M, Smith IE, Ebbs SR, Dixon JM, Skene A, A'Hern R, et al. Prognostic value of Ki67 expression after short-term presurgical endocrine therapy for primary breast cancer. J Natl Cancer Inst. 2007;99(2):167–70.
9. Ellis MJ, Tao Y, Luo J, A'Hern R, Evans DB, Bhatnagar AS, et al. Outcome prediction for estrogen receptor-positive breast cancer based on postneoadjuvant endocrine therapy tumor characteristics. J Natl Cancer Inst. 2008;100(19):1380–8.
10. Dehdashti F, Mortimer JE, Trinkaus K, Naughton MJ, Ellis M, Katzenellenbogen JA, et al. PET-based estradiol challenge as a predictive biomarker of response to endocrine therapy in women with estrogen-receptor-positive breast cancer. Breast Cancer Res Treat. 2009;113(3):509–17.
11. Juweid ME, Cheson BD. Positron-emission tomography and assessment of cancer therapy. N Engl J Med. 2006;354(5):496–507.
12. Weber WA, Ziegler SI, Thodtmann R, Hanauske AR, Schwaiger M. Reproducibility of metabolic measurements in malignant tumors using FDG PET. J Nucl Med. 1999;40(11):1771–7.
13. Ueda S, Tsuda H, Asakawa H, Shigekawa T, Fukatsu K, Kondo N, et al. Clinicopathological and prognostic relevance of uptake level using 18F-fluorodeoxyglucose positron emission tomography/computed tomography fusion imaging (18F-FDG PET/CT) in primary breast cancer. Jpn J Clin Oncol. 2008;38(4):250–8.
14. Young H, Baum R, Cremerius U, Herholz K, Hoekstra O, Lammertsma AA, et al. Measurement of clinical and subclinical tumour response using [18F]-fluorodeoxyglucose and positron emission tomography: review and 1999 EORTC recommendations. European Organization for Research and Treatment of Cancer (EORTC) PET Study Group. Eur J Cancer. 1999;35(13):1773–82.
15. Shankar LK, Hoffman JM, Bacharach S, Graham MM, Karp J, Lammertsma AA, et al. Consensus recommendations for the use of 18F-FDG PET as an indicator of therapeutic response in patients in National Cancer Institute Trials. J Nucl Med. 2006;47(6):1059–66.
16. Cascini GL, Avallone A, Delrio P, Guida C, Tatangelo F, Marone P, et al. 18F-FDG PET is an early predictor of pathologic tumor response to preoperative radiochemotherapy in locally advanced rectal cancer. J Nucl Med. 2006;47(8):1241–8.
17. Rousseau C, Devillers A, Sagan C, Ferrer L, Bridji B, Campion L, et al. Monitoring of early response to neoadjuvant chemotherapy in stage II and III breast cancer by [18F]fluorodeoxyglucose positron emission tomography. J Clin Oncol. 2006;24(34):5366–72.
18. Dose Schwarz J, Bader M, Jenicke L, Hemminger G, Janicke F, Avril N. Early prediction of response to chemotherapy in metastatic breast cancer using sequential 18F-FDG PET. J Nucl Med. 2005;46(7):1144–50.
19. Ueda S, Kondoh N, Tsuda H, Yamamoto S, Asakawa H, Fukatsu K, et al. Expression of centromere protein F (CENP-F) associated with higher FDG uptake on PET/CT, detected by cDNA microarray, predicts high-risk patients with primary breast cancer. BMC Cancer. 2008;8:384.
20. Kurosumi M, Akashi-Tanaka S, Akiyama F, Komoike Y, Mukai H, Nakamura S, et al. Histopathological criteria for assessment of therapeutic response in breast cancer (2007 version). Breast Cancer. 2008;15(1):5–7.
21. Tsuda H, Tani Y, Hasegawa T, Fukutomi T. Concordance in judgments among c-erbB-2 (HER2/neu) overexpression detected by two immunohistochemical tests and gene amplification detected by Southern blot hybridization in breast carcinoma. Pathol Int. 2001;51(1):26–32.
22. Tsuda H, Morita D, Kimura M, Shinto E, Ohtsuka Y, Matsubara O, et al. Correlation of KIT and EGFR overexpression with invasive ductal breast carcinoma of the solid-tubular subtype, nuclear grade 3, and mesenchymal or myoepithelial differentiation. Cancer Sci. 2005;96(1):48–53.
23. Ueda S, Tsuda H, Sato K, Takeuchi H, Shigekawa T, Matsubara O, et al. Alternative tyrosine phosphorylation of signaling kinases according to hormone receptor status in breast cancer overexpressing the insulin-like growth factor receptor type 1. Cancer Sci. 2006;97(7):597–604.
24. Allred DC, Harvey JM, Berardo M, Clark GM. Prognostic and predictive factors in breast cancer by immunohistochemical analysis. Mod Pathol. 1998;11(2):155–68.

25. Krainick-Strobel UE, Lichtenegger W, Wallwiener D, Tulusan AH, Janicke F, Bastert G, et al. Neoadjuvant letrozole in postmenopausal estrogen and/or progesterone receptor positive breast cancer: a phase IIb/III trial to investigate optimal duration of preoperative endocrine therapy. BMC Cancer. 2008;8:62.
26. Schelling M, Avril N, Nahrig J, Kuhn W, Romer W, Sattler D, et al. Positron emission tomography using [(18)F]fluorodeoxyglucose for monitoring primary chemotherapy in breast cancer. J Clin Oncol. 2000;18(8):1689–95.
27. Duch J, Fuster D, Munoz M, Fernandez PL, Paredes P, Fontanillas M, et al. 18F-FDG PET/CT for early prediction of response to neoadjuvant chemotherapy in breast cancer. Eur J Nucl Med Mol Imaging. 2009;36:1551–7.
28. Pons F, Duch J, Fuster D. Breast cancer therapy: the role of PET-CT in decision making. Q J Nucl Med Mol Imaging. 2009;53(2):210–28.
29. Kurosumi M, Takatsuka Y, Watanabe T, Imoto S, Inaji H, Tsuda H, et al. Histopathological assessment of anastrozole and tamoxifen as preoperative (neoadjuvant) treatment in postmenopausal Japanese women with hormone receptor-positive breast cancer in the PROACT trial. J Cancer Res Clin Oncol. 2008;134(6):715–22.
30. Tao Y, Klause A, Vickers A, Bae K, Ellis M. Clinical and biomarker endpoint analysis in neoadjuvant endocrine therapy trials. J Steroid Biochem Mol Biol. 2005;95(1–5):91–5.
31. Ellis MJ, Tao Y, Young O, White S, Proia AD, Murray J, et al. Estrogen-independent proliferation is present in estrogen-receptor HER2-positive primary breast cancer after neoadjuvant letrozole. J Clin Oncol. 2006;24(19):3019–25.

Oncogene (2011) 30, 4118–4128

www.nature.com/onc

ORIGINAL ARTICLE

MEK–ERK pathway regulates EZH2 overexpression in association with aggressive breast cancer subtypes

S Fujii[1], K Tokita[1], N Wada[2], K Ito[3], C Yamauchi[1], Y Ito[4] and A Ochiai[1]

[1]Pathology Division, Research Center for Innovative Oncology, National Cancer Center at Kashiwa, Kashiwa, Chiba, Japan; [2]Breast Surgery Division, National Cancer Center Hospital East, Kashiwa, Chiba, Japan; [3]Graduate School of Biomedical Sciences, Nagasaki University, Nagasaki, Japan and [4]Cancer Science Institute of Singapore, Proteos, Singapore

EZH2 overexpression occurs in various malignancies and is associated with a poor outcome. We have so far demonstrated that EZH2 downregulates the important genes such as *E-cadherin* and *RUNX3* by increasing histone H3K27 trimethylation. However, the mechanism of EZH2 overexpression in various cancer cells remains unclear. In this study we carried out a promoter analysis of the *EZH2* gene and investigated whether a survival signal that is upregulated in cancer cells is related to overexpression at the transcription level. We also explored the clinical relevance of the signaling pathway that leads to EZH2 overexpression in breast cancer and demonstrated that MEK–ERK1/2–Elk–1 pathway leads to EZH2 overexpression. The triple-negative and ERBB2-overexpressing subtypes of breast cancer are known to contain more rapidly proliferating breast cancer cells. The signaling pathway connected to EZH2 overexpression was associated with both aggressive subtypes of breast cancer. We show the significance that overexpression of histone modifier protein EZH2 in cancer cells and our study could pave the way for EZH2 inhibition to become an efficient treatment for more aggressive breast cancers.
Oncogene (2011) **30,** 4118–4128; doi:10.1038/onc.2011.118; published online 18 April 2011

Keywords: EZH2/MEK–ERK pathway; histone; triple negative; breast cancer; ERBB2-overexpressing breast cancer

Introduction

Enhancer of zeste homolog 2 (EZH2) is well known to be a histone modifier protein that functions as a methytransferase at lysine 27 of histone H3 (Cao *et al.*, 2002). EZH2 is also a member of the polycomb group of proteins and belongs to the polycomb repressive complex 2 (PRC2) subgroup (Schuettengruber *et al.*, 2007), and EZH2 has an important role in X-chromosome inactivation (Plath *et al.*, 2003). On the other hand, there have been several reports that overexpression of EZH2 occurs in various malignancies and that it is associated with a poor outcome in prostate cancer and breast cancer (Varambally *et al.*, 2002; Kleer *et al.*, 2003). In an attempt to determine the functional role of EZH2 overexpression in cancer tissue, we have already demonstrated that EZH2 downregulates important genes, such as *E-cadherin* and *RUNX3*, by increasing histone H3K27 trimethylation, which suggests that it may be an oncogene (Fujii *et al.*, 2008; Fujii and Ochiai, 2008). However, the mechanism of EZH2 overexpression in various cancer cells remains unclear. Although overexpression of EZH2 protein detected by immunohistochemical staining in various clinical tissue samples is associated with a poor outcome (Bachmann *et al.*, 2006), the mechanism responsible for the differences in rates of cancer cell positivity between individual cases also remains unclear.

Breast cancer is a heterogeneous disease with respect to outcome and response to treatment. The clinical course and treatment of breast cancer patients are to a large extent driven by the biological characteristics of their tumors, and accurate classification of breast cancers is of major importance. Expression of estrogen receptor (ER) or progesterone receptor (PgR) and epidermal growth factor receptor 2 (ERBB2) identified by immunohistochemical staining has long guided the classification of breast cancer, and the classification has proved useful in terms of predicting outcome and guiding treatment recommendations. Hormone receptor- (ER or PgR) positive breast cancers and ERBB2-positive breast cancers currently account for 75–80% and 15–20%, respectively, of all breast cancers. About half of ERBB2-positive cancers co-express hormone receptors (Slamon *et al.*, 1989; Konecny *et al.*, 2003), and the other 10–15% of breast cancers fall into the so-called triple-negative category, defined by the absence of expression of all three proteins. As a result, triple-negative breast cancers are resistant to existing targeted therapies, namely, trastuzumab and hormonal therapies. The pathways that drive proliferation of triple-negative breast cancer cells are still poorly understood. Five distinct subtypes of breast cancer, that is, a luminal subtype A, a luminal subtype B, an ERBB2-overexpressing subtype, a basal subtype and a normal

Correspondence: Dr A Ochiai, Pathology Division, Research Center for Innovative Oncology National Cancer Center at Kashiwa, 6-5-1, Kashiwanoha, Kashiwa, Chiba 277-8577, Japan.
E-mail: aochiai@east.ncc.go.jp
Received 16 July 2010; revised 3 March 2011; accepted 9 March 2011; published online 18 April 2011

breast-like subtype have been defined by RNA expression arrays (Perou *et al.*, 2000), and this classification has been refined by cytokeratin (CK) expression patterns. Although most basal-type breast cancers do not express ER, PgR or ERBB2 (Nielsen *et al.*, 2004), as a small number do, the overlap between basal-type breast cancer and triple-negative breast cancer is not complete. However, characteristically these tumors have a high mitotic count, scant stromal content, exhibit central necrosis, a pushing border of invasion, frequent apoptotic cells and a stromal lymphocytic response. The classification of breast cancers is clinically relevant because a higher proportion of patients with basal-type breast cancer have a poor outcome than patients with luminal type-breast cancer (Korsching *et al.*, 2008).

Previous studies have shown that increased expression of EZH2 is associated with aggressive behavior of breast cancers and a high breast cancer cell proliferation rate (Kleer *et al.*, 2003; Bachmann *et al.*, 2006). In this study we carried out a promoter analysis of the *EZH2* gene and investigated whether a survival signal that is upregulated in cancer cells is related to overexpression at the transcription level. We also explored the clinical relevance of the signaling pathway that leads to EZH2 overexpression in breast cancer.

Results

Promoter analysis

The −2874 to +599 (transcription start site designated as +1) long 5′ flanking region of *EZH2* was obtained by PCR amplification of human placenta genomic DNA. The fragment was then subcloned into the promoter-less luciferase reporter vector pGL3-Basic, and the putative promoter activity was measured by a dual-luciferase assay (Figure 1a). pGL3-Basic had basal strength in the form of luc+/Rluc activity, and that strength was set equal to 1. The deletion variants of the *EZH2* promoter region yielded different basal levels of expression of the luciferase gene. One of them, pGL3-696 exhibited about twofold increase in relative luciferase activity in

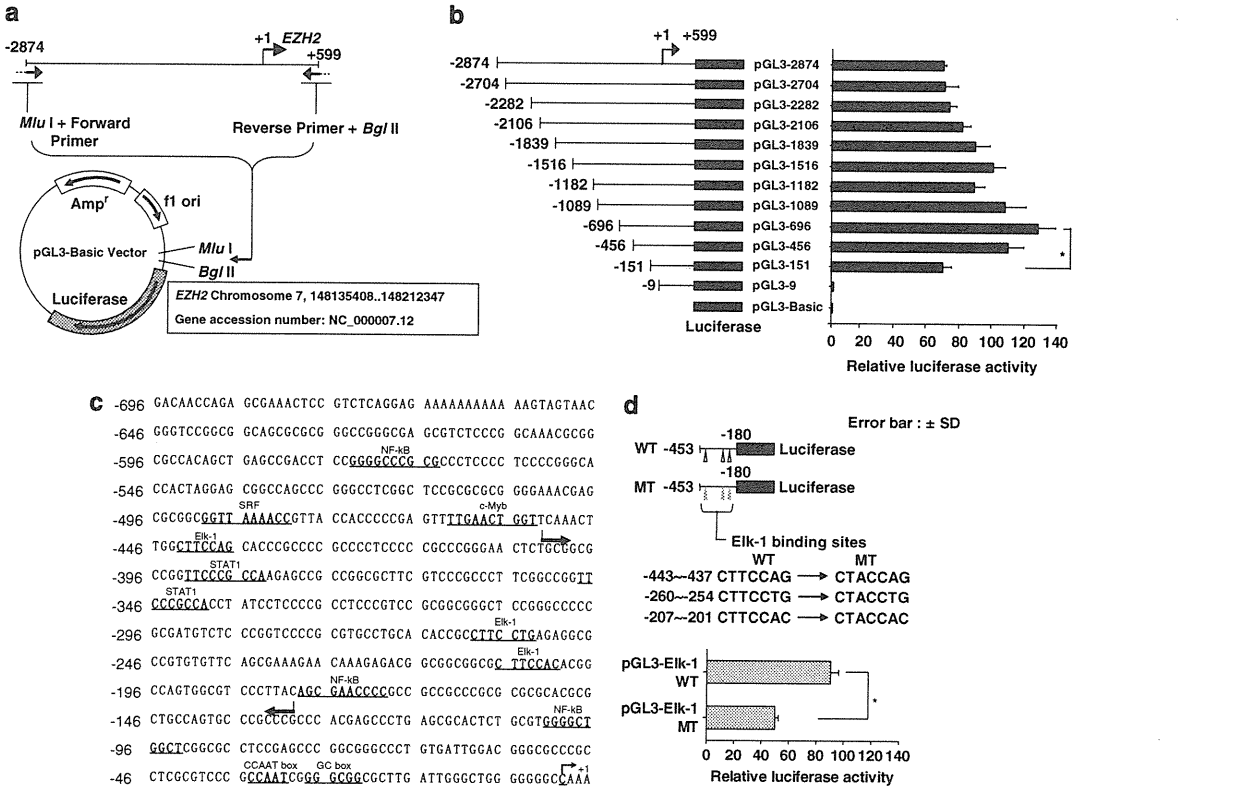

Figure 1 Promoter analysis of the *EZH2* promoter. (**a**) Construction of reporter plasmids with the *EZH2* promoter region and deletion variants inserted. The gene accession number is NC_000007.12. The reporter plasmid pGL3-2874 was constructed by inserting the PCR product of the putative *EZH2* promoter region into the MCS between the *Mlu*I and *Bgl*II sites of pGL3-Basic. +1 means the transcriptional start site. (**b**) Deletion variants of the *EZH2* promoter pGL3-2704, 2282, 2106, 1839, 1516, 1182, 1089, 696, 456 and 151 were derived from pGL3-2874. Asterisk mark focuses a difference of relative luciferase activity between pGL3-696 and pGL3-151 constructs. (**c**) Bioinformatic analysis of transcriptional factor binding sites in the *EZH2* 5′-flanking upstream region. Software was used to make the predictions. The numbers on the left side indicate the order upstream to the first base of the transcriptional start site. The transcription factors that bind to the region are labeled below their corresponding binding sites. The DNA sequence surrounded by two arrows was for mutation construct. (**d**) Three Elk-1 binding motifs were located within −453 nt and −180 nt. White and gray triangles indicate a wild or mutant sequence for Elk-1 binding motifs, respectively. WT, wild type; MT, mutant type.

comparison with that of pGL3-2874, and its activity was higher than that of the full-length promoter (pGL3-2874) (Figure 1b). A significant difference in relative luciferase activity between pGL3-696 and pGL3-151 was exhibited as about twofold difference between the deletion variants ($P<0.05$), and pGL3-151 displayed much lower relative luciferase activity than pGL3-696. We focused on the region responsible for the difference in relative luciferase activity and carried out a computational analysis with the TRANSFAC 6.0 software program (BIOBASE, Beverly, MA, USA; http://www.biobase-international.com/pages/index.php?id = transfac). The results revealed the expected enhancer sequences, such as CCAAT box and GC box, as well as transcription factor-binding sites. Within the −696 nt of the *EZH2* 5′ flanking region, there were three Elk-1 binding motifs, as well as many general transcription factors that constitute the basal transcription apparatus and response elements, including NF-κB, c-Myb, STAT1 and SRF (serum response factor), which is known to cooperate with Elk-1 for transcriptional activation (Figure 1c). There were three binding sites of Elk-1 between −696 nt and −151 nt of the *EZH2* 5′ flanking region (Figure 1d), suggesting that the MEK–ERK–Elk-1 pathway, which is known to be upregulated in various cancer cells, contributes to the EZH2 overexpression. Next, we made wild and mutant constructs with one point mutation for each Elk-1 binding sites. At first, wild and mutant DNA sequences of the *EZH2* promoter region encompassing the all three Elk-1 binding sites (the length is 274 bp) were synthesized, respectively, and inserted into pGL3-Basic Vector. Theafter, dual luciferase assays were carried out. The pGL3–Elk-1–MT exhibited almost a half decrease in relative luciferase activity compared with that of wild-type construct (Figure 1d). The decreased level was similar to the difference between deletion construct without three Elk-1 binding sites (pGL3-151) and pGL3–696 construct.

Effect of inhibition of the MEK–ERK–Elk-1 pathway on EZH2 expression

We proceeded to investigate whether inhibition of the MEK–ERK–Elk-1 pathway would affect EZH2 overexpression. First, the cytotoxic effect of the MEK inhibitor (U0126) on MDA-MB-231 cells was assessed by analyzing the cell growth curve. The results showed that the 40 μm concentration of the MEK inhibitor did not significantly affect cell survival, but as a higher concentration (400 μM) caused significant cell death, 40 μM was chosen as the optimal concentration to use in all experiments on MDA-MB-231 cells. The MDA-MB-231 cells were treated with 10 and 40 μM concentrations of the MEK inhibitor for 12 and 24 h, *EZH2* mRNA expression started to decrease at 12, and at 24 h it had reached one-third the level in the control (Figure 2a).

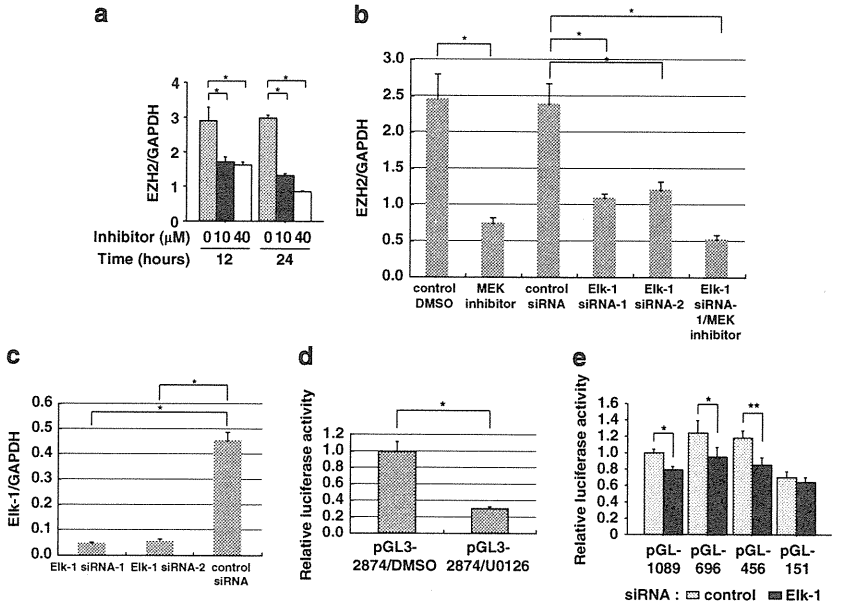

Figure 2 *EZH2* mRNA expression decreased after MEK inhibitor treatment and knockdown of Elk-1 in breast cancer cell line MDA-MB-231. (**a**) *EZH2* mRNA decreased after MEK inhibitor treatment (10 and 40 μM) at 12 and 24 h. (**b**) The level of *EZH2* mRNA decreased after MEK inhibitor treatment and knockdown by *Elk-1* siRNA transfection, and it decreased after a combination of MEK inhibitor treatment and *Elk-1* siRNA transfection. Two kinds of Elk-1 siRNAs (Elk-1 siRNA-1 and Elk-1 siRNA-2) were used to confirm the results. The *EZH2* mRNA expression levels were quantified by real-time RT–PCR. (**c**) The level of *Elk-1* after knockdown by siRNA transfection was also quantified by real-time RT–PCR. (**d**) After the transfection of pGL3-2874 constructed reporter plasmid and addition of MEK inhibitor at a concentration of 40 μM, MDA-MB-231 cells were incubated for 24 h and the reporter assays were carried out. (**e**) After the transfection of *Elk-1* siRNA, MDA-MB-231 cells were incubated for 24 h. Thereafter, four kinds of constructed reporter plasmids were transfected and incubated for 24 h, and the reporter assays were carried out. The results of the real-time RT–PCR and relative lucifierase activity are shown in the form of diagrams and the results were statistical analyses by Student's *t* test. *Indicates $P<0.05$, ** indicates $P<0.01$, and all data are means + s.d. of data from at least three experiments.

Knockdown of *Elk-1*, the functional transcription factor present in the downstream of the MEK–ERK pathway, by small interfering RNA (siRNA) transfection caused a decrease in level of *EZH2* mRNA expression that was similar to the decrease caused by MEK inhibitor treatment (Figure 2b). A combination of MEK inhibitor treatment and *Elk-1* siRNA transfection resulted in a decrease in level of *EZH2* mRNA expression that was almost the same as in response to treatment with the MEK inhibitor or *Elk-1* siRNA transfection alone (Figure 2b). The efficiency of *Elk-1* knockdown by siRNA transfection is shown in Figure 2c. We tested whether the MEK inhibitor treatment or *Elk-1* knockdown by siRNA transfection affected the relative luciferase activity of *EZH2* promoter. Both treatments affected the relative luciferase activity of *EZH2* promoter. However, in case that pGL3–151 constructed reporter plasmids without predicted Elk-1 binding sites was transfected, the relative luciferase activity of *EZH2* promoter was not affected by *Elk-1* knockdown (Figure 2e).

Phospho-Elk-1 binds to the promoter of EZH2

Computational analysis identified three Elk-1 binding sites within −696 nt of the *EZH2* 5′-flanking region (Figure 1c). We designed the three sets of PCR primers for the chromatin immunoprecipitation (ChIP) assay so that the amplified region would include or would not include Elk-1 binding sites (Figure 3a). We carried out the ChIP assay to determine whether phospho-Elk-1 or generic Elk-1 binds to a region of *EZH2* gene (Figure 3a). After treatment with the MEK inhibitor, the level of phospho-Elk-1 binding to the promoter region of the *EZH2* gene decreased significantly in comparison with the control ($P<0.05$) (Figures 3b and c), and it also decreased significantly in comparison with

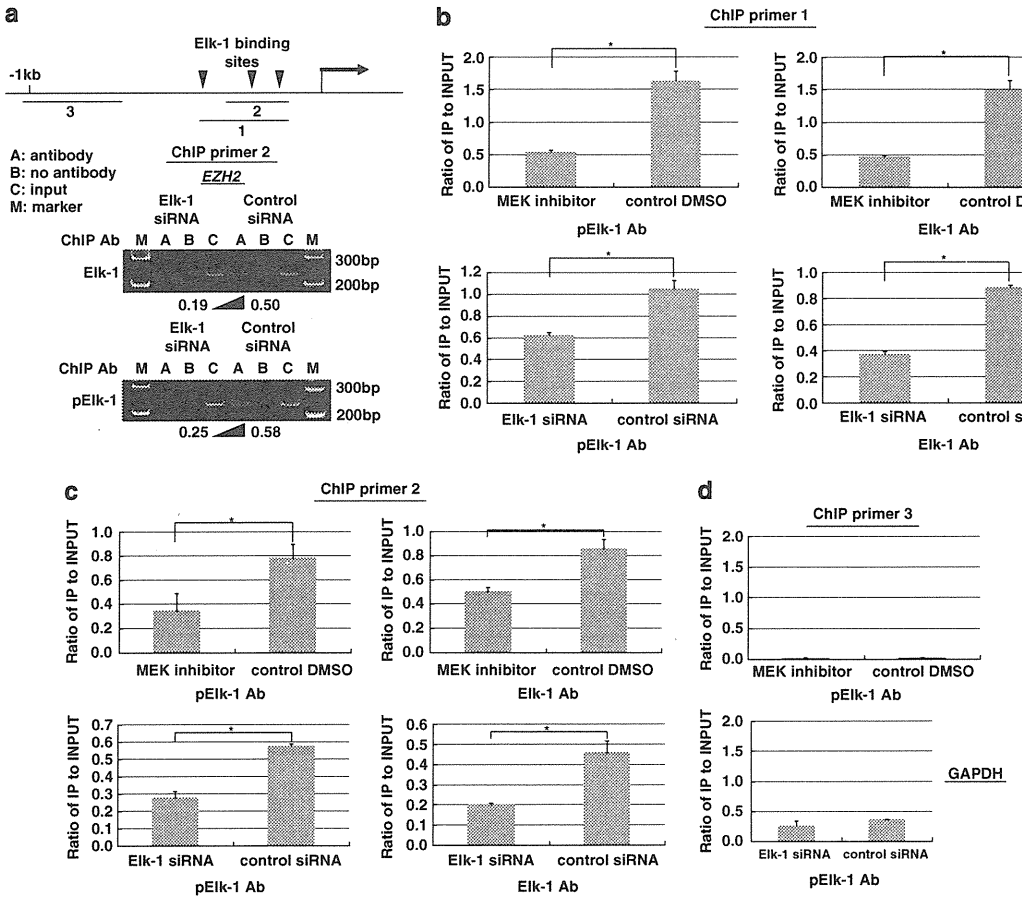

Figure 3 The decrease in *EZH2* mRNA expression after MEK inhibitor treatment and *Elk-1* knockdown was accompanied by a decreased level of phospho-Elk-1 binding to the *EZH2* promoter. (**a**) The three sets of primers for the ChIP assay were designed to encompass Elk-1 binding motif sites or not to encompass Elk-1 binding motif sites. The representative electrophoretic figures on 6%-acrylamide gel were shown and nonspecific immunoprecipitation was excluded. (**b**) ChIP primer 1. (**c**) ChIP primer 2. (**d**) ChIP primer 3 and ChIP primer for *GAPDH gene promoter*. ChIP assay was performed by using DNA–protein complex isolated from MDA-MB-231 cells treated with the MEK inhibitor for 24 h or transfected with *Elk-1* siRNA for 48 h, and immunoprecipitated with phospho-Elk-1 (pElk-1) or generic Elk-1 (Elk-1) antibody. The ratio of immunoprecipitated DNA to input DNA was quantified by performing a DNA 1000 assay with the Agilent 2100 bioanalyzer. Individual ChIP assays were carried out a total of at least three times to confirm the reproducibility of the PCR-based experiment. The results of the ChIP assays are shown in the form of diagrams and statistical analyses by Student's *t* test. *Indicates $P<0.05$, and all data are means + s.d. of data from at least three experiments.

the control after *Elk-1* siRNA transfection ($P<0.05$) (Figures 3b and c). The binding level of Elk-1 to the EZH2 promoter that was detected using a generic anti-Elk-1 antibody also decreased after MEK inhibitor treatment or Elk-1 knockdown (Figures 3b and c), which suggests that the generic anti-Elk-1 antibody used here recognizes phosphorylated Elk-1, as well as non-phosphorylated Elk-1. On the other hand, it was so difficult to detect signal intensity reflecting binding levels of phospho-Elk-1 to the *EZH2* promoter region without any predicted Elk-1 binding motif and to the non-targeted gene such as *GAPDH* by PCR-based method (Figure 3d). These results suggest that the level of phospho-Elk-1 binding to the *EZH2* promoter region with the predicted Elk-1 binding sites regulates the transcription of *EZH2* mRNA.

MEK–ERK–Elk-1 pathway regulates EZH2 protein expression in triple-negative and ERBB2-overexpressing breast cancer cell lines

The findings described thus far demonstrated the existence of MEK–ERK–Elk-1 pathway that functions as a regulator of *EZH2* mRNA overexpression in triple-negative breast cancer MDA-MB-231. In the next step, we investigated whether the pathway has a role in regulating EZH2 protein expression in the three different types of breast cancer cell lines, that is, the triple-negative/basal-type (MDA-MB-231 and MDA-MB-468), ERBB2 overexpressing/luminal B type (SKBr3), and hormone receptor-positive type (HCC1500). As shown in Figure 4a, the western blot analysis showed that MEK inhibitor (U0126) treatment decreased EZH2 protein expression in MDA-MB-231 cells. The decrease of EZH2 protein started 4 h after U0126 treatment and it was accompanied by a disappearance of phosphorylation of Elk-1. The decrease of EZH2 protein after U0126 treatment for 12 h was accompanied by a decrease in phosphorylation of both ERK1/2 and Elk-1 (Figure 4b). Knockdown of Elk-1 by siRNA transfection also decreased EZH2 protein expression and decreased Elk-1 of phosphorylation, without decreasing the phosphorylation level of pERK1/2, because Elk-1 is a downstream protein of the MEK–ERK1/2 pathway (Figure 4c). These results were the same as obtained in regard to *EZH2* mRNA after MEK

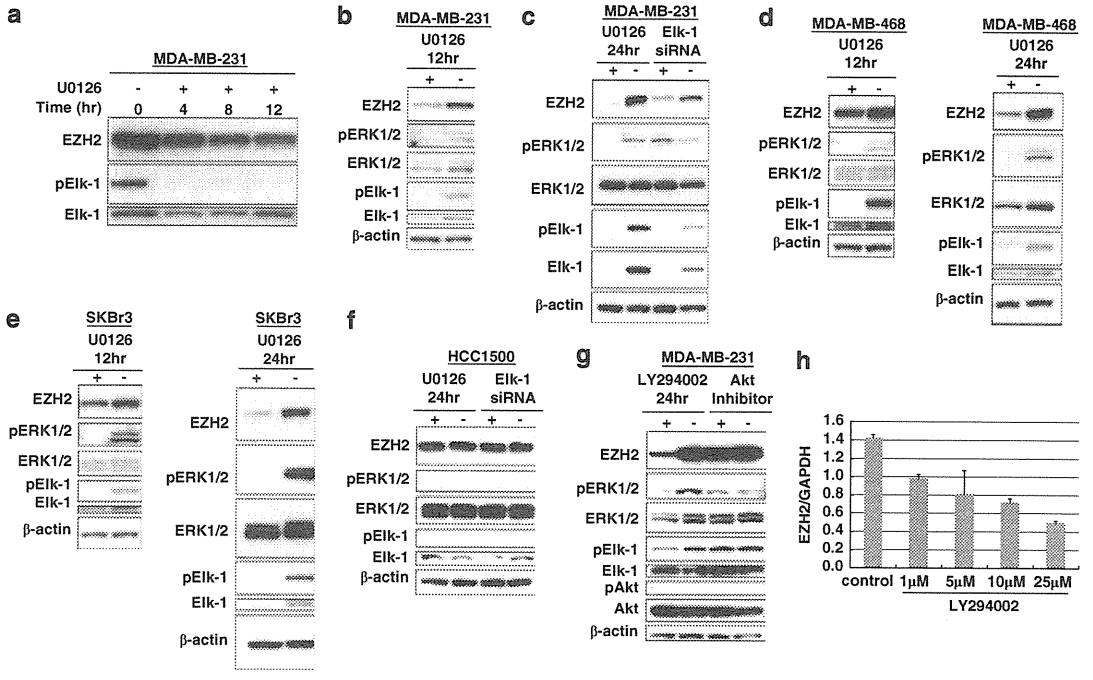

Figure 4 EZH2 protein expression after MEK inhibitor treatment and *Elk-1* siRNA transfection in triple-negative, ERBB2-overexpressing, hormone receptor-positive breast cancer cell lines assessed by western blot analysis. (**a**) Effects of U0126 treatment for 4, 8 and 12 h on Elk-1 phosphorylation, Elk-1 and EZH2 in MDA-MB-231 cells (triple-negative). (**b**) Effects of U0126 treatment for 12 h on EZH2, ERK1/2 phosphorylation, ERK1/2, Elk-1 phosphorylation and Elk-1 in MDA-MB-231 cells. (**c**) Effects of U0126 treatment and Elk-1 knockdown on EZH2, ERK1/2 phosphorylation, ERK1/2, Elk-1 phosphorylation and Elk-1 in MDA-MB-231 cells. Protein was extracted 24 h after MEK inhibitor treatment and 48 h after *Elk-1* siRNA transfection. (**d**) Effects of U0126 treatment for 12 and 24 h on EZH2, ERK1/2 phosphorylation, ERK1/2, Elk-1 phosphorylation and Elk-1 in MDA-MB-468 cells (triple-negative). (**e**) Effects of U0126 treatment for 12 and 24 h on EZH2, ERK1/2 phosphorylation, ERK1/2, Elk-1 phosphorylation and Elk-1 in SKBr3 cells (ERBB2-overexpressing). (**f**) Effects of U0126 treatment and Elk-1 knockdown on EZH2, ERK1/2 phosphorylation, ERK1/2, Elk-1 phosphorylation and Elk-1 in HCC1500 cells (hormone receptor-positive). Protein was extracted 24 h after MEK inhibitor treatment and 48 h after *Elk-1* siRNA transfection. (**g**) Effects of LY294002 (10 μM) or Akt inhibitor (20 μM) treatment on EZH2, ERK1/2 phosphorylation, ERK1/2, Elk-1 phosphorylation, Elk-1, Akt phosphorylation and Akt in MDA-MB-231 cells. Protein was extracted 24 h after MEK inhibitor treatment and 48 h after *Elk-1* siRNA transfection. (**h**) *EZH2* mRNA decreased after PI3K inhibitor treatment (1, 5, 10 and 25 μM) at 24 h in MDA-MB-231 cells.

inhibitor treatment and *Elk-1* siRNA transfection (Figure 2). MEK inhibitor treatment for 12 or 24 h decreased EZH2 protein expression in MDA-MB-468 cells and SKBr3 cells, and the decrease was also accompanied by a decrease in phosphorylation of both ERK1/2 and Elk-1 (Figures 4d and e), results that were similar to those observed in MDA-MB-231 cells. On the other hand, U0126 treatment or *Elk-1* knockdown by siRNA transfection did not have any effect on EZH2 expression in HCC1500 cells (Figure 4f). Next, we treated MDA-MB-231 cells with Akt inhibitor or PI3K inhibitor to determine the specificity of MEK inhibitor with respect to EZH2 expression. AKT inhibitor did not affect EZH2 expression, phospho-AKT was not detected in MDA-MB-231 cells by western blot analysis (Figure 4g), which was same as previous published data (Kenny *et al.*, 2007). *EZH2* mRNA expression also did not change after treatment with Akt inhibitor (Supplementary Figure 1). PI3K inhibitor (LY294002) did affect negatively EZH2 expression. PI3K inhibitor decreased the phosphorylation level of ERK1/2 and Elk-1 (Figure 4g), however, the decrease was not remarkable. The result of real-time reverse-transcription PCR (RT–PCR) showed that PI3K inhibitor decreased *EZH2* mRNA expression level (Figure 4h). These results suggest that PI3K inhibitor affect EZH2 expression negatively by downregulating MEK–ERK–Elk-1 pathway. The previous report shows that Rac exerts an effect downstream of PI3K to have enhancing role in regulation of the Raf/Erk signaling pathway downstream of Ras activated. PI3k inhibitor, LY294402 inhibited Erk activation by inhibiting Rac activation (Arai *et al.*, 2002). However, another downstream effector of PI3K may have a role in activation of Erk/Elk-1, further studies on signaling downstream of PI3K for regulation of EZH2 expression will be required to elucidate the molecular mechanisms.

EZH2 overexpression induced by the activated MEK–ERK1/2 pathway occurs in ERBB2-overexpressing and triple-negative breast cancer subtypes

We also explored the relevance of the signaling pathway that leads to EZH2 overexpression in breast cancer tissue. The result of immunohistochemical staining of the representative case with triple-negative breast cancer was shown in Figure 5. The cancer cells showed positivity for EGFR and pElk-1. The EZH2 that is supposed to be a downstream protein of MEK/ERK/Elk-1 pathway from the findings thus far demonstrated was overexpressed, and high MIB-1 index was also observed in the same area (Figures 5b–e). The two continuous and thin tissue sections showed the synchronized co-overexpression of EZH2 and pElk-1 proteins in individual cancer cells (Figures 5b and c). Among 178 breast cancer tissues, there was a significant correlation between EZH2 overexpression and breast cancer phenotype, the EZH2 protein expression positive rates of the ERBB2-overexpressing and triple-negative subtypes were much higher than that of the hormone receptor-positive subtype (Figure 6a). The percentages of cases classified as EZH2-overexpressing cases in the ERBB2-overexpressing subtype and triple-negative breast cancer subtype were much higher than in the hormone receptor-positive subtype (Figure 6b), suggesting that the MEK–ERK pathway mainly causes EZH2 overexpression in ERBB2-overexpressing and triple-negative breast cancer cells. In addition, the percentages of cases classified as RUNX3-negative or RUNX3-weakly expressed in cytoplasm in the triple-negative breast cancer subtype were much lower than in the hormone receptor-positive subtype (Figure 6c). We treated MDA-MB-231 cells with *Elk-1* siRNA transfection and examined whether the expression of *RUNX3* mRNA changed. As shown in Figure 6d, the expression of *RUNX3* mRNA started to increase 72 h after *Elk-1* knockdown.

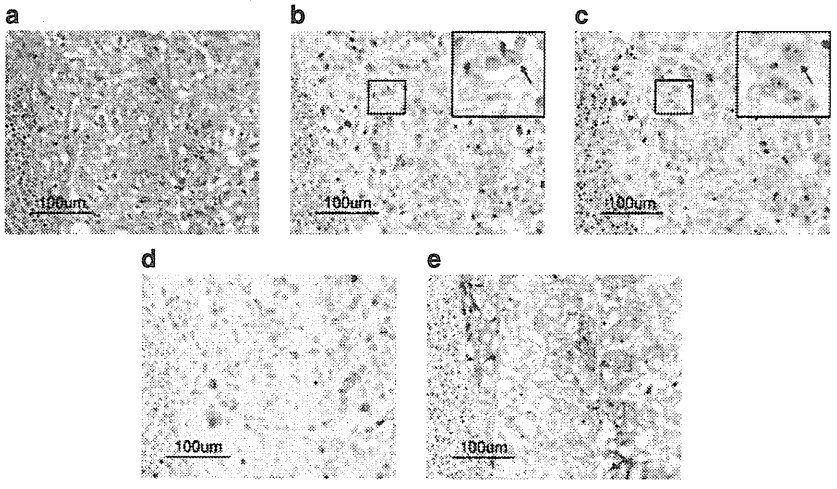

Figure 5 Immunohistochemical staining of breast cancer tissue of the triple- negative subtype. (**a**) H&E (hematoxylin and eosin), (**b**) EZH2, (**c**) pElk-1, (**d**) Ki-67 and (**e**) EGFR. Immunohistochemical stainings for EZH2 protein and pElk-1 protein were performed using the two continuous and thin tissue sections to show the positive correlation of expression of EZH2 protein and pElk-1 protein in individual cancer cells. The individual cancer cells surrounded by square box (marked by black arrow) were magnified to show the synchronized co-overexpression of EZH2 protein and pElk-1 protein.

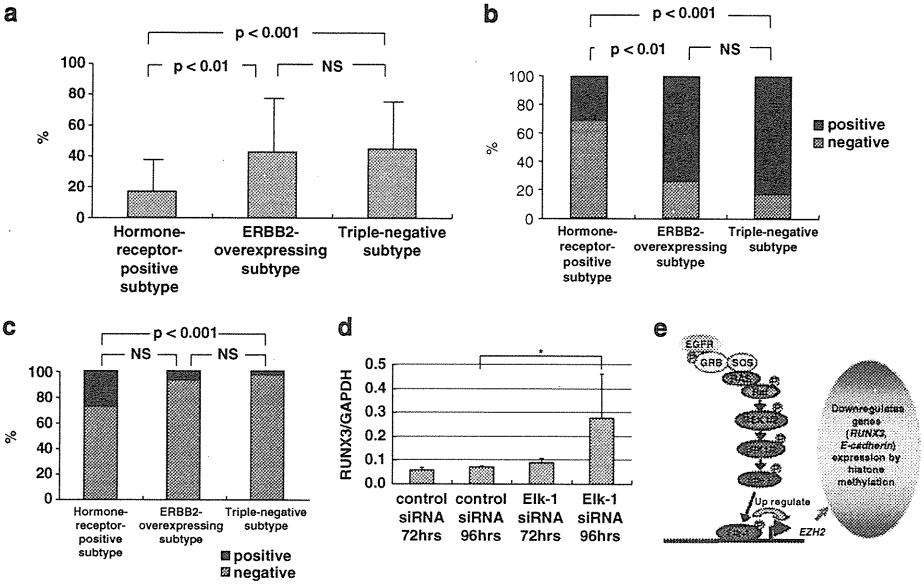

Figure 6 The relationship between EZH2 overexpression and three breast cancer subtypes. (**a**) EZH2 protein expression positive rates of the hormone receptor-positive subtype, ERBB2-overexpressing subtype and triple-negative subtype. The results of the positive rates of cancer cells are shown in the form of diagrams and statistical analyses by Kruskal–Wallis test followed by Dunn's method. All data are means + s.d. of data from all cases of each subtypes. NS; not significant by Dunn's method. (**b**) Percentages of cases with EZH2 overexpression among triple-negative, ERBB2-overexpressing and hormone receptor-positive breast cancers. The case with more than 10% positive cells for EZH2 protein expression is regarded as EZH2 overexpression case. The results of the percentages of cases with EZH2 overexpression of each subtypes are shown in the form of diagrams and statistical analyses by Kruskal–Wallis test followed by Dunn's method. NS; not significant by Dunn's method. (**c**) Percentages of cases with RUNX3-negativity or cytoplasmic RUNX3-weakly expression among triple-negative, ERBB2-overexpressing and hormone receptor-positive breast cancers. The results of the percentages of cases with RUNX3-negativity or cytoplasmic RUNX3-weakly expression of each subtypes are shown in the form of diagrams and statistical analyses by Kruskal–Wallis test followed by Dunn's method. NS; not significant by Dunn's method. (**d**) The level of *RUNX3* mRNA expression after *Elk-1* knockdown by siRNA transfection was quantified by real-time RT–PCR in MDA-MB-231 cells. *Indicates $P<0.05$, and all data are means + s.d. of data from at least three experiments. (**e**) Proposed pathway leading to EZH2 overexpression.

This result is similar to our previous result that RUNX3 expression is restored 72–96 h after knockdown of EZH2 (Fujii *et al.*, 2008). We would like to propose the signaling pathway leading to EZH2 overexpression in breast cancer cells (Figure 6e).

Discussion

The results of this study showed that the MEK–ERK–Elk-1 pathway, which is one of the signal transduction pathways that are upregulated in cancer cells, is linked to overexpression of EZH2, which is one of the histone modifier proteins. EZH2 has been reported to be overexpressed in various cancer cells (Raaphorst *et al.*, 2000; Varambally *et al.*, 2002; Kleer *et al.*, 2003; Bachmann *et al.*, 2006; Fujii and Ochiai, 2008; Fujii *et al.*, 2008), suggesting that the overexpression is caused by a variety of signals and pathways, some of which are specific to certain kinds of cancer cell and others of which are universal. The results provided evidence that Elk-1 is a critical factor downstream from ERK not only as a transcription factor for several other genes, but also for *EZH2*, resulting in chromatin remodeling at certain specific foci, such as *RUNX3* and *E-cadherin* (Fujii and Ochiai, 2008; Fujii *et al.*, 2008). We concluded that ERK has a pleiotropic role in gene regulation by controlling the phosphorylation of transcription factors, including Elk-1, and chromatin remodeling via EZH2 and histone H3 methylation. These effects seemed to be critical to the aggressiveness and high growth rate of triple-negative breast cancer (Figure 6). However, other transcriptional factors may bind to certain binding motifs in the *EZH2* promoter, and further experiments are needed to identify the factors that regulate EZH2 expression and are associated with the character of cancer cells, specifically with cancer cell phenotypes. The mechanism proposed here may be just one of several different mechanisms that impact EZH2 levels and function in cancer cells. There is precedent for microRNA regulation that affects both EZH2 mRNA and protein levels (Varambally *et al.*, 2008) and also non-coding RNA that can control EZH2 targeting in cancer cells (Gupta *et al.*, 2010). The comprehensive understanding of these multiple modes of controlling EZH2 expression is necessary and further studies are needed to clarify the connection of these modes related to cancer aggressive phenotypes such as invasiveness and metastasis.

The full-length reporter plasmid constructed did not exhibit the peak relative luciferase activity. A positive transcriptional effect of phospho-Elk-1 binding on the

promoter was shown in this study, but the longer deletion variants of the constructed reporter plasmid exhibited relative low luciferase activity, suggesting that there may be binding sites for repressive transcriptional factors in those regions of the *EZH2* promoter. The plausible possibility that *EZH2* transcription is regulated by a variety of transcriptional factors would suggest that histone modification by a histone modifier protein such as EZH2 may be reversible in response to several factors in the microenvironment, including inflammation, hypoxia and carcinogen exposure around normal or cancer cells. Histone modifier proteins are capable of the transcription of a whole set of genes simultaneously. Further study will be needed to devise a methodology for cancer treatment by regulating the expression of histone modifier proteins.

Western blot analyses of ERBB2-positive and triple-negative breast cancer cell lines were carried out to explore the extent of the inhibitory effect of MEK inhibitor treatment or Elk-1 knockdown on EZH2 protein expression (Figure 4). The remarkable effect of the MEK inhibitor on EZH2 protein in triple-negative and ERBB2-overexpressing cells suggests that the MEK/ERK pathway activated via *KRAS* mutation, EGFR amplification and ERBB2 amplification contribute strongly to EZH2 overexpression. In fact, MDA-MB-231 and MDA-MB-468 cells are *KRAS* mutant and EGFR amplified breast cancer cells, respectively (Hollestelle *et al.*, 2010). Tissue microarray studies have shown a high rate of EGFR overexpression in triple-negative breast cancers (Cleator *et al.*, 2007). In this study, the EZH2 protein expression positive rates of the ERBB2-overexpressing and triple-negative subtypes were much higher than that of the hormone receptor-positive subtype (Figure 6a). On the basis of the results of this study, we think that EZH2 inhibition is a critical treatment in triple-negative and ERBB2-overexpressing breast cancer cells.

Many phenotypical and molecular features, including ER negativity, high nuclear grade, high Ki-67 staining, CK5/6 expression, EGFR expression and *p53* mutation, are shared by sporadic triple-negative breast cancers and tumors that arise in carriers of the *BRCA1* mutation (Crook *et al.*, 1998; Sørlie *et al.*, 2001; Foulkes *et al.*, 2004). *BRCA1* is rarely mutated in sporadic breast cancers (Futreal *et al.*, 1994), however, the histopathological similarity of the two categories; triple-negative breast cancers and tumors with the *BRCA1* mutation leads us to speculate that common pathways may be associated with cancer cell proliferation. Interestingly, a recent study immunohistochemically demonstrated a clear increase in EZH2 protein levels in tumors from *BRCA1* mutation carriers (Puppe *et al.*, 2009). It also showed that *BRCA1*-deficient cancer cells are selectively dependent on their elevated EZH2 levels and that inhibition of EZH2 is about 20-fold more effective in killing *BRCA1*-deficient cells than in killing *BRCA1*-proficient mammary tumor cells, suggesting that EZH2 may be a target for drug therapy of a specific subtype of breast cancer. The results of our present study suggest that inhibition of EZH2 may critically block cancer cell proliferation in aggressive breast cancer phenotypes, including triple-negative breast cancers and BRCA1-deficient breast cancers.

The findings in this study showed that EZH2 overexpression was caused by activated MEK–ERK1/2-Elk-1 pathway. The signaling pathway connected to EZH2 overexpression is associated with aggressive phenotypes of breast cancer including triple-negative and ERBB2-overexpressing breast cancers. Our study could pave the way for EZH2 inhibition to become an efficient treatment for more aggressive breast cancers.

Materials and methods

Bioinformatic analysis and cloning of the EZH2 gene promoter region

By using the 5′ complementary DNA sequence of the *EZH2* gene as a probe, exons of the *EZH2* gene were identified as corresponding to the sequences of the nucleotides on human chromosome 7 (Gene Accession Number NC_000007. 12) by a BLAST search. The promoter and transcription binding sites on the 5′ flanking region of *EZH2* were predicted by conducting a TRANSFAC 6.0 analysis. The full-length *EZH2* gene promoter region from the 5′ flanking 2874-bp upstream region to 599-bp downstream region from the transcription starting site of the *EZH2* gene (148135408–148212347) was amplified by using human genomic placenta DNA (50 ng/μl) as a template and a PCR primer with an incorporated *Mlu*I site (EZH2−2874), and a primer with an incorporated *Bgl*II site (EZH2 + 599R) (Supplementary Table 1). The PCR product after digestion with *Bgl*II and *Mlu*I was inserted into the pGL3-Basic vector (Promega, Madison, WI, USA), and the entire length of the inserted PCR product was sequenced by using an ABI PRISM 3100 Genetic Analyzer (Applied Biosystems, Carlsbad, CA, USA) and the designed sequence primers (Supplementary Table 1).

Construction of recombinant luciferase reporter plasmids with the full-length EZH2 gene promoter region, deletion variants and mutation variant

The whole *Bgl*II–*Mlu*I fragment of the recombinant plasmid was subcloned into the *Bgl*II–*Mlu*I site of the MCS of the pGL3-Basic vector (Promega), and the plasmid obtained was designated as pGL3-2874. Several deletion variants designated as pGL3-2704, pGL3-2282, pGL3-2106, pGL3-1839, pGL3-1516, pGL3-1182, pGL3-1089, pGL3-696, pGL3-456, pGL3-151 and pGL3-9 were generated using primer sets of the forward primer with an incorporated *Mlu*I site or the reverse primer with an incorporated *Bgl*II site (Supplementary Table 1) as described above. The wild and mutant DNA sequences of the *EZH2* promoter region encompassing all the three Elk-1 binding sites (−453 nt to −180 nt) were synthesized, respectively and inserted into pGL3-Basic Vector. The wild-type and mutant-type constructs were designated as the pGL3–Elk-1–WT and pGL3–Elk-1–MT, respectively. T was replaced into A in each Elk-1 binding motif of pGL3–Elk-1–MT construct.

Cell culture and transfection of reporter plasmids

Human breast cancer cell line MDA-MB-231 was routinely grown in RPMI medium containing 10% fetal bovine serum and 10% glutamine. The reporter plasmids were transfected with Lipofectamine 2000 (Invitrogen, Camarillo, CA, USA).

Dual-luciferase reporter assay

Dual-luciferase reporter assays with the constructed reporter plasmids were carried out according to the manufacturer's

instructions (Promega). pRL-SV40 plasmid (Promega) was co-transfected to normalize the transfection efficiency. Transfections were carried out on 12-well plates, and the reporter assays were carried out on 96-well plates. Briefly, 4 h after transfection, the cell culture medium was replaced with fresh complete growth medium, and the cells were incubated for another 20 h. The activity of firefly (*Photinus pyralis*) and Renilla (*Renilla reniformi*) luciferases (luc+ and Rluc, respectively) in cell lysates was measured sequentially with a 96-well plate luminometer (Luminescencer-JNR AB-2100, Atto Bio-Instrument, Tokyo, Japan). Promoter strength was expressed as luc+ activity/Rluc activity.

Breast cancer cell lines

Three breast cancer cell lines, that is, MDA-MB-231, MDA-MB-468, SKBr3, and HCC1500, all obtained from the American Type Culture Collection (Manassas, VA, USA), were maintained at 37 °C in RPMI supplemented with 10% heat-inactivated fetal bovine serum and 1% glutamine under a 5% CO_2 atmosphere. MDA-MB-231 and MDA-MB-468 are basal-type breast cancer cell lines, which are defined by triple negativity for ER, PgR and ERBB2. SKBr3 cells are characterized by ERBB2 expression, HCC1500 cells are characterized by hormone-receptor expression (Hollestelle *et al*., 2010).

RNA isolation and real-time RT–PCR

Total RNA from the cell lines was isolated with TRIzol Reagent (Invitrogen) and reverse transcribed to complementary DNA with ExScript RT Reagent (Takara, Yokkaichi, Mie, Japan). Real-time RT–PCR was carried out with specific primers for *EZH2* and *Elk-1* and a Smart Cycler (Cepheid, Sunnyvale, CA, USA). *GAPDH* expression was used to normalize for variance. Real-time fluorescence monitoring of the PCR products was performed with SYBR Green I fluorescent dye (Takara). The levels of expression of specific genes are reported as ratios to the level of expression of *GAPDH* in the same master reaction. The PCR primer pairs (5′ to 3′) used for each gene were: *EZH2*, CCCTGACCTCTG TCTTACTTGTGGA and ACGTCAGATGGTGCCAGCA ATA; *Elk-1*, CACTTCTGGAGCACCCTGAGTC and AGA GGCCATCCACGCTGATA; and *GAPDH*, GCACCGTCA AGGCTGAGAAC and ATGGTGGTGAAGACGCCAGT. These primer sets were designed by Takara.

MEK inhibitor, PI3K inhibitor and Akt inhibitor treatment

MDA-MB-231 cells were treated with a MEK inhibitor (U0126) (Promega) at a concentration of 40 μM for 4, 8, 12 and 24 h, and the other cell lines, including MDA-MB-468 and SKBr3 cells, were treated with the MEK inhibitor at 50 μM. MDA-MB-231 cells were treated with a PI3K inhibitor (LY294002) (Calbiochem, Darmstadt, Germany) or an Akt inhibitor (Akt inhibitor V, Triciribine) (Calbiochem) at a concentration of 1, 5, 10, 25, 50 μM for 24 h. Total RNA from the treated cell lines was then isolated and used for real-time RT–PCR for *EZH2*, *Elk-1* and *GAPDH*, ChIP assay and western blot analysis.

RNA interference

Two 21-nucleotide duplex siRNA for *Elk-1* and one negative control siRNA were synthesized by Ambion (Carlsbad, CA, USA), Inc. (*Elk-1* siRNA ID, s4634; *Elk-1* siRNA-1 and s4633; *Elk-1* siRNA-2), and 24 h after plating the cells they were transfected with *Elk-1* siRNA or control siRNA by using the DharmaFECT transfection reagent (Dharmacon, Lafayette, CO, USA) according to the manufacturer's instructions. Cells were harvested 48 h after transfection and subjected to several assays, including real-time RT–PCR, ChIP assay and western blot analysis.

Chromatin immunoprecipitation assay

The ChIP assay was carried out as previously described (Fujii *et al*., 2003). The PCR conditions for the *EZH2* gene (Gene Accession Number NC_000007.12) promoter, which contains or does not contain Elk-1 biding motifs, were applied with the following three primer pairs: ChIP primer 1 which contains three Elk-1 binding motifs (5′ to 3′): TTAAAACCGTTACCA CCCCCGAGTTTTGAA and TTCGCTGTAAGGGACGCC ACTGGCCGTGT, ChIP primer 2 which contains two Elk-1 binding motifs (5′ to 3′): AACTCTGCGGCGCCGGTT CCCGCCAAGA and TTCGCTGTAAGGGACGCCACTG GCCGTGT and ChIP primer 3 which does not contain any Elk-1 binding motifs (5′ to 3′): ACGAACAGTGGA AGGGTCTG and GGAGTTTCGCTCTGGTTGTC. A ChIP primer pair for *GAPDH* as negative control for Elk-1 binding was used (5′ to 3′): CACCGTGTGCCCAAGACCTC and CAGCCCTGTAGCCTGGACCT (Morris *et al*., 2005). A 5 μg amount of antibody was used in this assay. The antibodies used were phospho-Elk-1 and generic (pan-reactive) Elk-1 antibody purchased from Spring Bioscience (Pleasanton, CA, USA). Individual ChIP assays after treatment with the MEK inhibitor and *Elk-1* siRNA transfection were carried out at least three times to confirm the reproducibility of the PCR-based experiment. Preliminary PCR reactions were carried out to determine the optimal PCR conditions to assure linear amplification of the DNA. To measure the level of phospho-Elk-1 or generic Elk-1 binding in each immunoprecipitate, the ratios of immunoprecipitated DNA to input DNA were calculated by measuring the intensity of the PCR product in immunoprecipitated DNA versus input DNA (total chromatin) amplified by PCR in a linear range. The ratios were calculated using the PCR products by performing a DNA 1000 assay with the Agilent 2100 bioanalyzer and using DNA chips for electrophoresis (Agilent Technologies, Santa Clara, CA, USA).

Western blot analysis

Cells were lysed with whole-cell lysis buffer (80 mM glycerophosphate, 20 mM EGTA, 15 mM $MgCl_2$, 20 mM NAF, 150 mM NaCl, 1 mM EDTA, 0.5% NP-40, 10 mM Na_3VO_4, 1 mM phenylmethylsulfonyl fluoride and a protease inhibitor tablet (Roche, Mannheim, Germany), and the lysates were frozen in liquid nitrogen and thawed three times to rupture the cell membranes. Samples of the lysates were incubated for 30 min on ice to lyse the nuclei and then centrifuged at 8900 rpm. The protein concentration of each sample was determined with a BCA Protein Asssay Kit (Pierce, Rockford, IL, USA). Equal amounts of protein (20 μg) from each cell line were subjected to western blot analysis. The probing antibodies were EZH2 antibody (1:1000) (BD Transduction Laboratories, Sparks, MD, USA), phospho-p44/42 MAPK (ERK1/2) antibody (1:1000) (Cell Signaling Technology, Boston, MA, USA), p44/42 MAPK (ERK1/2) antibody (1:1000) (Cell Signaling Technology), phospho-Elk-1 antibody (1:200) (Santa Cruz, Santa Cruz, CA, USA), Elk-1 antibody (1:200) (Santa Cruz), Akt antibody (1:1000) (Cell Signaling Technology), pAkt antibody (Ser 473) (Cell Signaling Technology), and β-actin antibody (1:50) (Santa Cruz).

Breast cancer tissue samples

A total of 178 breast cancer specimens that had been histologically diagnosed as invasive ductal carcinoma were studied and classified into three types: a hormone receptor-positive type (ER- and/or PgR-positive), an ERBB2-

overexpressing type (ERBB2-overexpressing with/without hormone-receptor-positive) and triple-negative type (hormone receptor-negative and ERBB2 not overexpressed). All specimens were obtained from females (mean age 58.3 years; s.d. ± 11.1) by surgical resection at the National Cancer Hospital East, and the histological diagnosis was carried out by routine microscopic analysis of sections of formalin-fixed, paraffin-embedded specimens. None of the patients had received any preoperative treatment, including radiation therapy, hormone therapy or chemotherapy. A representative section that included the maximum diameter of the tumor was used for the immunohistochemical analysis. All clinicopathological data were according to the TNM classification (UICC) and obtained from the clinical and pathology records. Several clinicopathological factors were shown in Supplementary Table 2.

Immunohistochemical staining

The breast cancer tissues were used for the immunohistochemical analysis. Immunohistochemistry for EZH2 (1:25) (BD Transduction Laboratories), phospho-Elk-1 (1:25) (Spring Bioscience), MIB-1 (1:50) (Dako, Tokyo, Japan), EGFR (1:50) (Novocastra, New Castle, UK) and RUNX3 (1 μg/ml) (R3-6E9) (Ito *et al.*, 2005) was carried out on sections of formalin-fixed, paraffin-embedded tissue by microwave-induced epitope retrieval and with the Dako Envision detection system. Appropriate positive and negative internal controls were used to validate immunohistochemical staining.

Conflict of interest

The authors declare no conflict of interest.

Acknowledgements

We wish to acknowledge the assistance of Ms Hiroko Hashimoto for cell culture support and the assistance of Mr Shinya Yanagi for making paraffin-embedded thin sections for immunohistochemistry. The research described in this report has been funded by a grant from the Ministry of Education, Culture, Sports, Science and Technology, Japan (21590453), to SF. Individual contributions of each author; Study concept and design; SF, AO, Acquisition of data; SF, KT, Analysis and interpretation of data; SF, KT, NW, Drafting the manuscript; SF, Critical revision of the manuscript for important intellectual content; SF, KI, YI, AO. Statistical analysis; SF, KT, NW Obtained funding; SF, Material support; NW, KI, YI, CY, Study supervision; SF.

References

Arai A, Kanda E, Miura O. (2002). Rac is activated by erythropoietin or interleukin-3 and is involved in activation of the Erk signaling pathway. *Oncogene* **21**: 2641–2651.

Bachmann IM, Halvorsen OJ, Collett K, Stefansson IM, Straume O, Haukaas SA *et al.* (2006). EZH2 expression is associated with high proliferation rate and aggressive tumor subgroups in cutaneous melanoma and cancers of the endometrium, prostate, and breast. *J Clin Oncol* **24**: 268–273.

Cao R, Wang L, Wang H, Xia L, Erdjument-Bromage H, Tempst P *et al.* (2002). Role of histone H3 lysine 27 methylation in Polycomb-group silencing. *Science* **298**: 1039–1043.

Cleator S, Heller W, Coombes RC. (2007). Triple-negative breast cancer: therapeutic options. *Lancet Oncol* **8**: 235–244.

Crook T, Brooks LA, Crossland S, Osin P, Barker KT, Waller J *et al.* (1998). p53 mutation with frequent novel condons but not a mutator phenotype in BRCA1- and BRCA2-associated breast tumours. *Oncogene* **17**: 1681–1689.

Foulkes WD, Brunet JS, Stefansson IM, Straume O, Chappuis PO, Bégin LR *et al.* (2004). The prognostic implication of the basal-like (cyclin E high/p27 low/p53 + /glomeruloid-microvascular-proliferation +) phenotype of BRCA1-related breast cancer. *Cancer Res* **64**: 830–835.

Fujii S, Ito K, Ito Y, Ochiai A. (2008). Enhancer of zeste homologue 2 (EZH2) down-regulates RUNX3 by increasing histone H3 methylation. *J Biol Chem* **283**: 17324–17332.

Fujii S, Luo RZ, Yuan J, Kadota M, Oshimura M, Dent SR *et al.* (2003). Reactivation of the silenced and imprinted alleles of ARHI is associated with increased histone H3 acetylation and decreased histone H3 lysine 9 methylation. *Hum Mol Genet* **12**: 1791–1800.

Fujii S, Ochiai A. (2008). Enhancer of zeste homolog 2 downregulates E-cadherin by mediating histone H3 methylation in gastric cancer cells. *Cancer Sci* **99**: 738–746.

Futreal PA, Liu Q, Shattuck-Eidens D, Cochran C, Harshman K, Tavtigian S *et al.* (1994). BRCA1 mutations in primary breast and ovarian carcinomas. *Science* **266**: 120–122.

Gupta RA, Shah N, Wang KC, Kim J, Horlings HM, Wong DJ *et al.* (2010). Long non-coding RNA HOTAIR reprograms chromatin state to promote cancer metastasis. *Nature* **464**: 1071–1076.

Hollestelle A, Nagel JH, Smid M, Lam S, Elstrodt F, Wasielewski M *et al.* (2010). Distinct gene mutation profiles among luminal-type and basal-type breast cancer cell lines. *Breast Cancer Res Treat* **121**: 53–64.

Ito K, Liu Q, Salto-Tellez M, Yano T, Tada K, Ida H *et al.* (2005). RUNX3, a novel tumor suppressor, is frequently inactivated in gastric cancer by protein mislocalization. *Cancer Res* **65**: 7743–7750.

Kenny PA, Lee GY, Myers CA, Neve RM, Semeiks JR, Spellman PT *et al.* (2007). The morphologies of breast cancer cell lines in three-dimensional assays correlate with their profiles of gene expression. *Mol Oncol* **1**: 84–96.

Kleer CG, Cao Q, Varambally S, Shen R, Ota I, Tomlins SA *et al.* (2003). EZH2 is a marker of aggressive breast cancer and promotes neoplastic transformation of breast epithelial cells. *Proc Natl Acad Sci USA* **100**: 11606–11611.

Konecny G, Pauletti G, Pegram M, Untch M, Dandekar S, Aguilar Z *et al.* (2003). Quantitative association between HER-2/neu and steroid hormone receptors in hormone receptor-positive primary breast cancer. *J Natl Cancer Inst* **95**: 142–153.

Korsching E, Jeffrey SS, Meinerz W, Decker T, Boecker W, Buerger H. (2008). Basal carcinoma of the breast revisited: an old entity with new interpretations. *J Clin Pathol* **61**: 553–560.

Morris DP, Michelotti GA, Schwinn DA. (2005). Evidence that phosphorylation of the RNA polymerase II carboxyl-terminal repeats is similar in yeast humans. *J Biol Chem* **280**: 31368–31377.

Nielsen TO, Hsu FD, Jensen K, Cheang M, Karaca G, Hu Z *et al.* (2004). Immunohistochemical and clinical characterization of the basal-like subtype of invasive breast carcinoma. *Clin Cancer Res* **10**: 5367–5374.

Perou CM, Sørlie T, Eisen MB, van de Rijn M, Jeffrey SS, Rees CA *et al.* (2000). Molecular portraits of human breast tumours. *Nature* **406**: 747–752.

Plath K, Fang J, Mlynarczyk-Evans SK, Cao R, Worringer KA, Wang H *et al.* (2003). Role of histone H3 lysine 27 methylation in X inactivation. *Science* **300**: 131–135.

Puppe J, Drost R, Liu X, Joosse SA, Evers B, Cornelissen-Steijger P *et al.* (2009). BRCA1-deficient mammary tumor cells are dependent on EZH2 expression and sensitive to Polycomb Repressive Complex 2-inhibitor 3-deazaneplanocin A. *Breast Cancer Res* **11**: R63.

Raaphorst FM, van Kemenade FJ, Blokzijl T, Fieret E, Hamer KM, Satijn DP *et al.* (2000). Coexpression of BMI-1 and EZH2 polycomb group genes in Reed-Sternberg cells of Hodgkin's disease. *Am J Pathol* **157**: 709–715.

Schuettengruber B, Chourrout D, Vervoort M, Leblanc B, Cavalli G. (2007). Genome regulation by polycomb and trithorax proteins. *Cell* **128**: 735–745.

Slamon DJ, Godolphin W, Jones LA, Holt JA, Wong SG, Keith DE *et al.* (1989). Studies of the HER-2/neu proto-oncogene in human breast and ovarian cancer. *Science* **244**: 707–712.

Sørlie T, Perou CM, Tibshirani R, Aas T, Geisler S, Johnsen H *et al.* (2001). Gene expression patterns of breast carcinomas distinguish tumor subclasses with clinical implications. *Proc Natl Acad Sci USA* **98**: 10869–10874.

Varambally S, Cao Q, Mani RS, Shankar S, Wang X, Ateeq B *et al.* (2008). Genomic loss of microRNA-101 leads to overexpression of histone methyltransferase EZH2 in cancer. *Science* **322**: 1695–1699.

Varambally S, Dhanasekaran SM, Zhou M, Barrette TR, Kumar-Sinha C, Sanda MG *et al.* (2002). The polycomb group protein EZH2 is involved in progression of prostate cancer. *Nature* **419**: 624–629.

Supplementary Information accompanies the paper on the Oncogene website (http://www.nature.com/onc)

The Breast 20 (2011) 431–436

Contents lists available at ScienceDirect

The Breast

journal homepage: www.elsevier.com/brst

Original article

Radiofrequency ablation of early breast cancer followed by delayed surgical resection – A promising alternative to breast-conserving surgery

Shoichiro Ohtani [a,*,h], Mariko Kochi [a,*,h], Mitsuya Ito [a], Kenji Higaki [a], Shinichi Takada [b], Hiroo Matsuura [b], Naoki Kagawa [c], Sakae Hata [d], Noriaki Wada [e], Kouki Inai [f], Shigeru Imoto [g], Takuya Moriya [d]

[a] Department of Breast Surgery, Hiroshima City Hospital, 7-33 Moto-machi, Naka-ku, Hiroshima 730-8518, Japan
[b] Department of Pathology, Hiroshima City Hospital, 7-33 Moto-machi, Naka-ku, Hiroshima 730-8518, Japan
[c] Kagawa Breast Clinic. 1–20 Mikawa-cho, Naka-ku, Hiroshima 730-0029, Japan
[d] Department of Pathology 2, Kawasaki Medical University, 577 Matsushima, Kurashiki, Okayama 701-0192, Japan
[e] Department of Breast Surgery, National Cancer Center Hospital East, 6-5-1 Kashiwanoha, Kashiwa, Chiba 277-8577, Japan
[f] Department of Pathology, Graduate School of Biomedical Sciences, Hiroshima University, 1-2-3 Kasumi, Minami-ku, Hiroshima 734-8551, Japan
[g] Department of Breast Surgery, School of Medicine, Kyorin University, 6-20-2 Shinkawa, Mitaka, Tokyo 181-8611, Japan

ARTICLE INFO

Article history:
Received 7 December 2010
Received in revised form
29 March 2011
Accepted 16 April 2011

Keywords:
Radiofrequency ablation
Early breast cancer
Complete tumour cell death

ABSTRACT

To examine the radiofrequency ablation (RFA) reliability in early breast cancer, we performed RFA followed by delayed surgical resection on 41 patients with invasive or non-invasive breast carcinoma less than 2 cm. MRI scans were obtained before ablation and resection. Excised specimens were examined pathologically by haematoxylin-eosin and nicotinamide adenine dinucleotide-diaphorase staining. 40 patients completed 1 RFA session, which was sufficient to achieve complete tumour cell death. Overall complete ablation rate was 87.8% (36/41). There were no treatment-related complications other than that of a superficial burn in 1 case. After RFA, the tumour was no longer enhanced on MRI in 25/26 (96.2%) cases. Residual cancer, which was suspected on MRI in 1 case, was confirmed pathologically. MRI could be an applicable modality to evaluate therapeutic effect. RFA could be an alternate local treatment option to breast-conserving surgery for early breast cancer.

Introduction

Early breast cancer treatment has evolved over the past decade. Currently, there has been a trend towards less-invasive approaches in the local treatment of breast cancer. Breast-conserving surgery has largely replaced mastectomy for primary breast cancer, as several large randomized trials have shown no survival difference between the 2 surgical options.[1–3] Conventional axillary lymph node dissection has been replaced with sentinel lymph node biopsy for clinically node-negative breast cancer, which affords improved staging and minimal morbidity.[4,5] With these fundamental changes in the breast cancer treatment strategy, there is an impetus to replace the less-invasive surgery with ablation techniques that eliminate the primary tumour without surgery. Several modalities enable minimally invasive ablation of the primary tumour, such as cryosurgery, laser ablation, thermoablation, and high-intensity focused ultrasound, but radiofrequency ablation (RFA) appears to be the most promising technique.

One major goal in breast-conserving treatment is to preserve a cosmetically acceptable breast. Since cosmetic results are related, to some extent, to the tissue amount removed, treating a tumour without resection has great appeal. Progress in detection methods, such as magnetic resonance imaging (MRI) and widespread application of screening mammography, will increase the detection of very small, non-palpable tumours, which further emphasizes the need for minimally invasive methods to achieve local tumour destruction. RFA is gaining acceptance as a treatment modality for several tumour types, but not yet for primary breast cancer, as there is yet insufficient evidence for its use as a standard therapy, in particular with regard to complete tumour cell death within the whole ablated area.

The current study was undertaken to determine the feasibility of treating early breast cancer with RFA and to evaluate tumour cell death and marginal clearance of ablated area by pathological study. Goals of this study were to examine the RFA reliability as a local treatment option in early breast cancer patients instead of breast-conserving surgery.

* Corresponding authors. Tel.: +81 82 221 2291; fax: +81 82 223 5514.
E-mail addresses: sho_ohtani@hotmail.com (S. Ohtani), mariko-leigh-k@live.jp (M. Kochi).
[h] S. Ohtani and M. Kochi contributed equally to this work.

0960-9776/$ – see front matter © 2011 Elsevier Ltd. All rights reserved.
doi:10.1016/j.breast.2011.04.007

Materials and methods

Enrolment

Forty-one patients, with pathologically proven invasive or non-invasive breast carcinoma less than 2 cm and clinically lymph node negative, were enrolled in this pilot study, conducted between March 2007 and February 2009. Core needle biopsy or vacuum-assisted biopsy was performed to determine tumour grade, lymphovascular invasion, hormone receptor status and HER2/neu status. The other inclusion criteria were as follows: tumour easily imaged by ultrasound and lumpectomy planed as the initial treatment. Exclusion criteria included more than 1 tumour in the same breast and the presence of extensive suspicious microcalcifications surrounding the tumour mass. Patients with pacemakers, sensitivity to lidocaine or coagulopathy, or who were pregnant or lactating were also excluded. Pre-treatment evaluation consisted of a complete history and physical examination, pathological review of the carcinoma and laboratory evaluation including a complete blood count and coagulation profile. Furthermore, bilateral mammography, enhanced breast MRI and positron emission tomography-CT were performed within 2 months of RFA. This study was approved by the institutional review board at Hiroshima City Hospital. All enrolled patients were informed about this study and signed a written consent for participation.

Breast ultrasound

Bilateral breast imaging was performed to include the known tumour and surrounding breast tissue using a 7.5 mHz transducer (EUB-5500; TOSHIBA, Japan). Three-dimensional tumour measurements were performed and recorded.

Breast MRI scans

Breast MRI scans were performed before ablation and within 48 h before surgical resection. The 3-T system (Signa; G.E. Medical Systems, Japan) was utilized. Patients were imaged in the prone position with a dedicated double breast coil. Axial and sagittal T1- and T2-weighted images were obtained by the following protocol: (1) axial, T1-weighted spin-echo (500–700/16–17 [repetition time in milliseconds/echo time in milliseconds]) sequence with a 32–36 cm field of view, 3 mm section, 1 mm gap, and 512 × 256 matrix for both breasts; (2) axial, T2-weighted fast spin-echo with fat saturation sequence of the affected breast, 12–18 cm field of view, 3 mm section, 1 mm gap, and 128 or 192 matrix; and (3) sagittal T1-weighted spin-echo with fat saturation sequence after the intravenous gadodiamide administration (0.5 M, Omniscan; Nycomed, Japan). A 20 ml gadodiamide bolus was administered, regardless of body weight, followed by a 20 ml physiological saline bolus. Imaging was initiated during saline injection.

Radiofrequency ablation

RFA was performed under either general anaesthesia or local anaesthesia and sedation. In the local anaesthesia group, intravenous sedation with midazolam titrated doses were administered in preparation for RFA. Under local anaesthesia and sedation, sentinel lymph node biopsy was first performed, then, under ultrasound guidance, 0.5% lidocaine was injected around the tumour. For analgesia, a sufficient volume of lidocaine injected over the pectoralis major is important. A small skin incision was made with a number 11 surgical blade. A 3 cm Cool-Tip RF Needle Electrode (Valleylab, Boulder, CO, USA) was inserted at the centre of the tumour under ultrasound guidance. For prevention of skin burn, 5% glucose liquid with a higher electrical resistance than saline was injected between the skin and tumour to increase the space between. The needle electrode was attached to a 500 kHz monopolar RF generator capable of producing 200 W. Grounding was achieved by attaching 2 grounding pads to the patient's thighs before the procedure. Tissue impedance was monitored continuously using circuitry incorporated in the generator. Radiofrequency energy was applied only once not exceeding 15 min. Power was set at 5 W and increased by 10 W intervals every 1 min until a rapid increase in impedance occurred (so-called roll-off). For prevention from skin burn, a sterile ice bag was placed on the skin over the ablated area. The core temperature of the ablated area was measured immediately after roll-off. Under general anaesthesia, the abovementioned procedure was performed but without using lidocaine and midazolam.

Surgery

Breast-conserving surgery (Bp 1.5 cm) was performed immediately after RFA (immediate surgical resection) under general anaesthesia or 1–2 months after RFA (delayed surgical resection) under local anaesthesia.

Pathological evaluation

After the specimen removal, pathological evaluation with haematoxylin-eosin (HE) staining was performed to evaluate the therapeutic effect according to the response criteria of the Japanese Breast Cancer Society[6] and to estimate the tumour size and marginal status. Moreover, to accurately evaluate tumour cell death, histochemical analysis of tumour viability with nicotinamide adenine dinucleotide-diaphorase (NADH) staining was performed.[7]

Follow up

Decisions regarding adjuvant chemotherapy or hormonal therapy were made based on the pre-treatment tumour size measured by breast MRI. Axillary lymph node metastasis was determined by sentinel lymph node biopsy results. Furthermore, prognostic indications such as estrogen receptor status, progesterone receptor status, HER2/neu status, lymphovascular invasion and grade were determined by pre-treatment core biopsy. According to each patient's risk category, adjuvant therapy was administered in all patients. Whole breast irradiation was also performed in every case.

Results

Patient characteristics

Of the 41 patients in this pilot study, 9 initially underwent breast-conserving surgery immediately after RFA under general anaesthesia (immediate surgical resection). RFA was subsequently performed under local anaesthesia and sedation in the remaining 32, following which breast-conserving surgery was performed under local anaesthesia 1–2 months after RFA (delayed surgical resection). All but 1 patient completed 1 RFA session. Patient characteristics are summarized in Table 1 (median tumour size as assessed by enhanced MRI scan, 13 mm [range, 5–18 mm]; median volume of 0.5% lidocaine administered, 42 ml [range, 32–55 ml]; median RFA application time, 9 min [range, 6–15 min]; median tumour core temperature immediately after RFA, 85 °C [range, 64–100 °C]). There were no treatment-related complications other than that of a superficial burn in 1 case right above the ablated area.

Table 1
Characteristic of patients and primary tumour characteristics ($n = 41$).

	No. of cases
Age (years)	
Range	38–92
Median	59
Tumour size on MRI	
Median (mm)	13
< 10 mm	6
10 mm >=	35
Histology	
IDC	36
DCIS	5
Tumour grade	
1	26
2	3
3	2
ER	
+	38
–	3
PgR	
+	35
–	6
HER2	
+	1
–	40
Anaesthesia	
General	9
Local	32
Ablation time (minutes)	
Range	6–15
Median	9
Core temperature (°C)	
Range	65–100
Median	85
Complication	
Superficial skin burn	1
None	40

IDC, invasive ductal carcinoma.
DCIS, non-invasive ductal carcinoma.

Breast MRI imaging

On post-RFA MRI scans, 25/26 studies (96.2%) in which the patient had pre-RFA enhancement displayed no residual enhancement of the breast lesion. In 1 case (3.8%), in which intolerable pain prevented completion of 1 RFA session, post-MRI scans demonstrated residual enhancement consistent with residual invasive and intraductal tumour, which was confirmed histologically. Therefore, a post-ablation MRI scan appears to predict therapeutic effect by RFA for breast cancer. An ablation zone, characterized by altered signal intensity and architectural distortion, with a minor degree of peripheral enhancement was easily visible in all cases. This ablation zone measured 3.0–6.1 cm at its greater diameter (median, 3.7 cm) and 1.8–5.5 cm at its lesser diameter (median, 2.5 cm). We termed this peripheral enhancement the protein degenerative ring, within which NADH staining demonstrated complete cell death. Representative pre- and post-RFA MRI scans demonstrating successful ablation and the protein degenerative ring are shown in Fig. 1. Residual cancer, which was suspected on MRI in 1 case, was confirmed pathologically (Fig. 2).

Pathological evaluation

HE staining of the ablated lesion removed immediately after RFA could not demonstrate complete tumour cell death, because cancer cell was diagnosed as viable cell only by HE staining. According to the response criteria of the Japanese Breast Cancer Society,[6] no pathological complete response (Grade 3) was observed in specimens removed immediately after RFA; however, it was observed in 4 (12.5%) specimens removed by delayed surgical resection. As times elapses after ablation, tumour cell death in a tissue sample by delayed surgical resection could be more easily diagnosed than in resection immediately after RFA. However, even in delayed surgical resection specimens, HE staining alone could not reveal all pathological complete cell death (Table 2). Therefore, to evaluate more accurate tumour cell death, NADH staining was performed in specimens from 12 patients, in all (100%) of whom no viable cancer cells (i.e., complete cell death) within the whole ablated area and surgical margins were demonstrated. Of these 12 cases, only 2 showed complete pathological response by HE staining (Table 3). Therefore, NADH staining is indispensable for evaluating tumour cell death, even in delayed surgical resection specimens. The macroscopic and histological findings are shown in Fig. 3. In 5 cases, complete histological ablation could not be achieved, with only non-invasive components remaining in 4 cases. Complete ablation was indicated on imaging examination in these 4 cases, yet pathological evaluation revealed residual non-invasive ductal cancer outside the degenerative protein ring. This may indicate the limitations of imaging-based diagnosis (in particular with regard to the extent of ductal spread, accurate diagnosis of which is not easy). Invasive and non-invasive components were found in 1 case (Fig. 2), where uncontrolled pain resulted in treatment failure. Adequate analgesia is also essential for successful ablation. Overall, a complete ablation rate of 87.8% (36/41) was observed, based on the findings of HE and NADH staining.

Discussion

Various thermal ablation treatments have been attempted for breast cancer, including cryosurgery,[8] laser ablation,[9] MR-guided

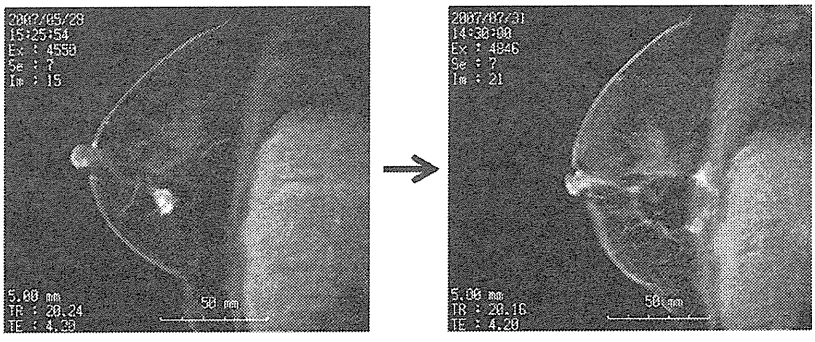

Fig. 1. Enhanced MRI scans demonstrate successful RFA ablation. An irregular, enhancing lesion is observed in the pre-RFA image. After RFA, the tumour is no longer enhanced. A zone of ablation within the protein degenerative ring is demonstrated.

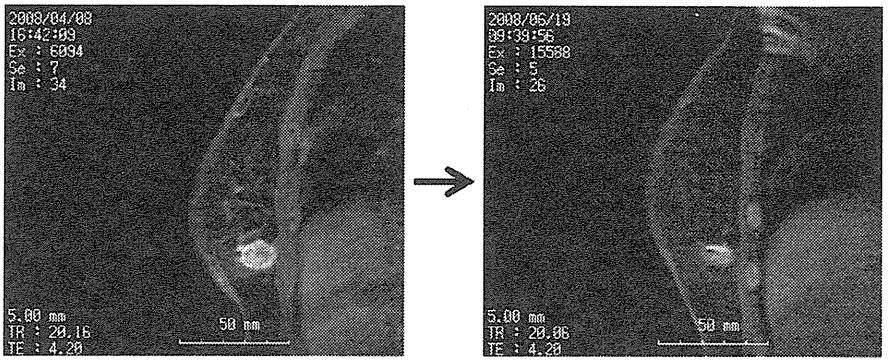

Fig. 2. The post-RFA MRI demonstrates residual enhancement consistent with a residual invasive and intraductal tumour, which was confirmed histologically.

high-intensity focused ultrasound[10] and RFA. Although each of these offers theoretical advantages, each also carries significant disadvantages. Cryoablation, requiring expensive and often bulky equipment, appears to be less effective because of incomplete freezing and a subsequent high rate of residual disease. Laser ablation is not effective for larger areas and requires another probe to measure temperature. MR-guided focused ultrasound also requires very expensive and extensive equipment; moreover it takes a few hours for a single treatment.

RFA for breast cancer appears to be the most promising modality. Many investigators have attempted feasibility studies on RFA followed by resection, as shown in Table 4, whose results support RFA use in localized breast cancer treatment.[11–21]

Our study was designed to gain further evidence on RFA reliability.

This study investigated delayed surgical resection performed 1–2 months after RFA to better assess tumour cell death over the entire ablated area; most RFA feasibility studies have investigated resection performed immediately after RFA, although 1 study reported on delayed surgical resection undertaken 1–3 weeks after RFA.[11] At the beginning of our study, we also performed immediate resection after RFA, however, pathological HE evaluation failed to demonstrate tumour cell death within the ablated zone. A delay in resection facilitates more physiological assessment. Therefore, we decided to excise the ablated area 1–2 months after RFA. To our best knowledge, no report has estimated tumour cell death in specimens resected 1–2 months after RFA. In specimens examined 1–2 months after RFA, complete tumour cell death could not be demonstrated by HE staining alone, whereas this was demonstrated by NADH staining in same specimens. NADH staining is easy and reliable in this study field. Interestingly, the cell nuclei disappearance was observed both from the centre and the ablated zone periphery by HE staining, and a cell death area was clearly demarcated from the surrounding viable tissue by a band of foam cells, which we termed the protein degenerative ring. Following resection of the ablated area 6 months after RFA, all cell nuclei in that area will disappear; complete tumour cell death may be demonstrated by HE staining alone if resection is performed over 6 months after RFA.

Another feature of this study is that RFA was performed under local anaesthesia and sedation as day surgery, a protocol that was extremely well tolerated, successful in eradicating tumours and which may point the way forward. Adequate analgesia over the pectoralis major is important in RFA, and no complications occurred, apart from the 1 case where intolerable pain obviated successful completion. On post-RFA MRI scanning, this patient had residual enhancement consistent with invasive and intraductal residual tumour, which was confirmed histologically. RFA performance under local anaesthesia by day surgery is ideal for minimally invasive treatment for breast cancer, which was one of our aims.

According to a predetermined standardized algorithm, radiofrequency energy was often applied more than once in breast cancer, but several investigators have implied that a single application is sufficient.[14,15,18] Our results are concomitant with their view for achieving complete tumour cell death within the whole ablated area, and are thus significant. Excess ablation leads to side effects such as skin burn, and multiple sessions require increased analgesia levels, which run contrary to performing RFA as day

Table 2
Histological analysis of ablated area by RFA.

Resection immediately after RFA (9 cases)	Delayed surgical resection (32cases)
Grade 1a: 4 cases (44.4%)	Grade 1a: 1 case (3.1%)
Grade 1b: 1 case (11.1%)	Grade 1b: 6 cases (18.8%)
Grade 2: 2 cases (22.2%)	Grade 2: 21 cases (65.6%)
Grade 3: 0 case (0%)	Grade 3: 4 cases (12.5%)
unknown: 2 cases (22.2%)	

Evaluation by response criteria of Japanese Breast Cancer Society

Response criteria of Japanese Breast Cancer Society	
Grade 0	No response Almost no change in cancer cells alter treatment
Grade 1	Slight response
Grade 1a	Mild response Mild change in cancer cell regardless of the area, or marked changes in cancer cell seen in less than one third of cancer cells
Grade 1b	Moderate response Marked changes in one third or more but less two thirds of tumor cells
Grade 2	Marked response Marked changes in two thirds or more of tumor cells
Grade 3	Complete response Necrosis or disappearance of all tumor cells. Replacement of all cancer cells by granuloma-like and/or fibrous tissue, In the case of complete dassapearance of cancer cells, pre-treatment pathological evidence of the presence of cancer is necessary

Table 3
Comparison of pathological evaluation by NADH and HE staining.

NADH staining	HE staining
No viable cell: 12 cases (100%)	Grade 1a: 0 case (0%)
Viable cell: 0 case (0%)	Grade 1b: 1 case (8.3%)
	Grade 2: 9 cases (75%)
	Grade 3: 2 cases (16.6%)